

Dynamics and evolutionary status of the young triple stellar system, TY Coronae Austinae

H. Beust^{1,2}, P. Cororon¹, L. Siess¹, M. Forestini¹, and A-M. Lagrange^{1,2}

¹ Laboratoire d'Astrophysique de l'Observatoire de Grenoble, B.P. 53, F-38041 Grenoble Cedex 9, France

² Institut d'Astrophysique de Paris, CNRS, 98 bis boulevard Arago, F-75014 Paris, France

Received 5 June 1996 / Accepted 2 September 1996

Abstract. The young star TY CrA was known as an eclipsing binary, which surprisingly appeared circularized but not synchronized. Recently, a third companion was detected, orbiting at roughly 1 A.U. from the central binary, on a significantly eccentric and inclined orbit. The dynamics of this triple system is here investigated, on the basis of the tentative fits of the tertiary orbit. We show that according to pure 3-body dynamics, the TY CrA central binary should be subject to periodic changes related to the so-called Kozai mechanism in cometary dynamics, which should lead to a rapid collapse. Adding tidal effects within that binary actually prevents it from collapsing. We also show that thanks to the combination of tidal effects and 3-body dynamics, the rotation axes of the components of the central binary may be locked in a particular position (in the orbital plane) which might explain the apparent non-synchronism of the binary. Such a situation would not be stable if the central binary was alone. The calculations are performed using interior models of the stars depending on their age. We show that the particular position is only stable if the system is less than a few 10^6 yrs old, i.e. if the secondary is a pre-main sequence star, otherwise the binary synchronizes. Hence we constrain the age of this system, which is in agreement with the conclusion reached from the comparison with evolutionary tracks.

Key words: stars: TY CrA – binaries: close – stars: rotation – stars: evolution – celestial mechanics

1. Introduction

The Herbig star TY CrA has been known as a short period eclipsing binary ($P=2.889$ days; Kardopolov et al. 1981) and a spectroscopic binary of type SB2 (Lagrange et al. 1993, hereafter Paper I). The identification of the radial velocity curves of both components allowed to determine their masses ($\sim 3.0 M_{\odot}$ and

$\sim 1.6 M_{\odot}$ respectively), together with their orbital characteristics (Cororon et al. 1994, hereafter Paper II). $v \sin i$ measurements toward both components gave also access to their rotation velocities, assuming their rotation axes is perpendicular to their orbital plane, i.e., to the line of sight. While the $1.6 M_{\odot}$ secondary appears marginally synchronized, the $3.0 M_{\odot}$ is surprisingly sub-synchronous (Paper II). The binary is thus almost circularized ($e \simeq 0.02$), but not synchronized. As pointed out by Casey et al. (1993), this cannot be explained straightforwardly, since in any case, tidal effects are expected to synchronize the rotation of the stars before circularizing the orbit. In fact, Hut (1981) showed that this holds for any system where the angular orbital momentum is initially significantly larger than the rotational one, which is the case most of the time, and in particular for TY CrA. In any case, a strong sub-synchronism of the $3.0 M_{\odot}$ primary is hard to explain. This led Casey et al. (1993) to suggest that the rotation axes of both components might not be perpendicular to the orbital plane of the binary, although there seemed to be no obvious argument supporting this assumption.

Perhaps the most recent advance concerning the TY CrA system is the detection of a third component orbiting the original binary system (Casey et al. 1995; Cororon et al. 1995, hereafter Paper III). In Paper III, we presented tentative fits of the orbital motion of the tertiary around the center of mass of the binary system, based on heliocentric velocity measurements. The five possible solutions are listed in Table 1. The referential frame ($Oxyz$) used to define the angular orbital elements is chosen so that the origin coincides with the center of mass of the whole system, and that the (Oz) axis points towards the Earth. Solutions #1 and #2 actually achieve the best fit.

The five solutions present in fact remarkable common features:

- a semi-major axis of the order of 1 A.U., with an orbital period significantly less than 1 year;
- a rather high eccentricity (four solutions have $e \simeq 0.5$);
- a tertiary mass $m_3 \simeq 1.2 - 1.4 M_{\odot}$, although this parameter is weakly constrained (large uncertainty);
- an inclination $i \simeq 16 - 25^{\circ}$.

Send offprint requests to: H. Beust

Table 1. Different solutions for the orbit of the tertiary

Parameter	Solution #1	Solution #2	Solution #3	Solution #4	Solution #5
Orbital period (days)	270 ± 1.35	268 ± 1.28	239 ± 1.68	145 ± 0.48	126 ± 0.17
Semi-major axis (a) (A.U.)	1.47 ± 0.06	1.46 ± 0.06	1.37 ± 0.06	0.98 ± 0.04	0.89 ± 0.04
Eccentricity (e)	0.507 ± 0.086	0.500 ± 0.087	0.266 ± 0.13	0.445 ± 0.17	0.538 ± 0.16
Argument of periastron (ω) ($^\circ$)	153 ± 16	155 ± 17	188 ± 24	227 ± 14	232 ± 14
Inclination (i) ($^\circ$)	20 ± 3	20 ± 3	24 ± 5	20 ± 3	16 ± 3
Tertiary mass (M_\odot)	1.26 ± 0.57	1.25 ± 0.57	1.44 ± 0.59	1.38 ± 0.58	1.21 ± 0.57

The orbit appears thus eccentric, and highly inclined with respect to that of the binary: assuming that the close binary is an eclipsing system, its inclination with respect to the plane of the sky should be close to 90° . The obtained values for the inclination of the orbit of the tertiary show therefore that this orbit is inclined by 65 or 70° with respect to that of the eclipsing binary.

The similarities between the relevant solutions found for the orbit of the tertiary allow us to assume that it is significantly constrained, and that it is eccentric and inclined with respect to that of the binary.

Such an unusual configuration for a triple system is not surprising and is observed in other hierarchical multiple systems as well (Hale 1994). The triple star Algol (Lestrade et al. 1993) is indeed a triple system with a similar spatial configuration.

The detection of the third component allows us to reconsider the sub-synchronism problem of the central binary. The purpose of this paper is to investigate the dynamics of the TY CrA system on the basis of the fit solutions of Table 1, combining 3-body dynamics with tidal effects inside the binary. As we will see below, this study helps us putting constraints on the evolutionary status of TY CrA. Hence, we precise in Sect. 2 the present constraints on the evolutionary status of TY CrA obtained from its location in the Hertzsprung-Russell diagram (hereafter HRD). In Sect. 3, we investigate the role of pure 3-body dynamics within the TY CrA system. In Sect. 4, we review and compare the various tidal mechanism able to act within the central binary. In Sect. 5, we add them to the 3-body dynamics, showing that the stability of the central binary is actually ensured by tidal effects. In Sect. 6, we perform long-term calculations of the TY CrA system, taking into account the fact that the stars do evolve during the integration. We interpret our results in Sect. 7, showing that the apparent sub-synchronism of the $3.0 M_\odot$ could correspond to a particular equilibrium location of its rotation axis, thanks to the role of the third companion. Our conclusions are presented in Sect. 8.

2. Evolutionary status of TY CrA triple system

From previous photometric, spectroscopic and dynamical computations, we have already learned that the $3.0 M_\odot$ primary of the TY CrA system has a total luminosity $80 L_\odot < L_1 < 100 L_\odot$ and effective temperature $10\,500\text{K} < T_{\text{eff},1} < 11\,450\text{K}$ (see Paper I). Note that, as the other components of the TY CrA system are much less massive, the luminosity of the whole system is dominated by the first component. The location of this component in the HRD normally allows to determine its total mass m_1

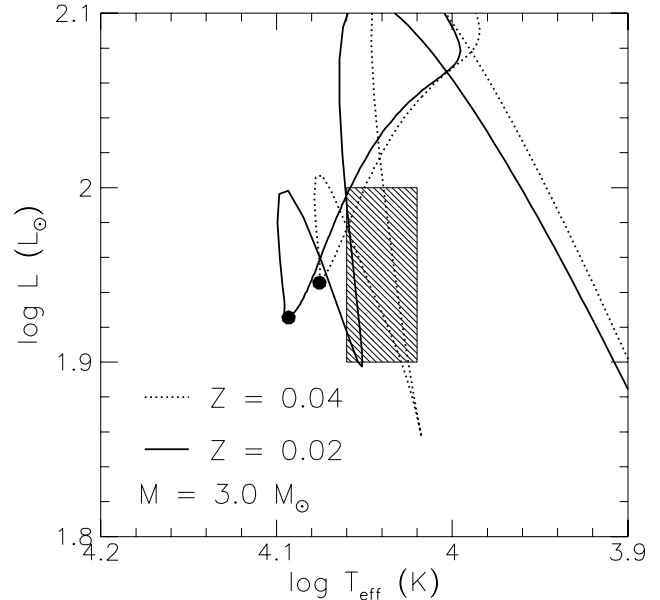


Fig. 1. Hertzsprung-Russell diagram showing computed evolution tracks for $M = 3 M_\odot$ and $Z = 0.02$ (solid line) or 0.04 (dashed line), as well as the observed position of the first TY CrA component taking account of the observational uncertainties

and age t , by comparison with computed evolutionary tracks. However, the HRD location of such theoretical tracks also depends on the metal content of the modeled stars, most currently pointed out by the metallicity Z , i.e., the total mass fraction of all the elements but hydrogen and helium. Unfortunately, we do not have yet a precise determination of the TY CrA metallicity. However, as TY CrA consists in a very young triple stellar system, it appears reasonable to assume, on grounds of our knowledge of the galactic chemical evolution, that its metallicity is quite similar or larger than the solar one, namely $Z \geq 0.02$. This leads to $2.9 M_\odot \leq M_1 \leq 3 M_\odot$, in agreement with the determination based on the velocity curves (see Paper II). In Fig. 1, we illustrate that mass determination by showing $3 M_\odot$ theoretical tracks (corresponding to $Z = 0.02$ and 0.04) together with the observational box for TY CrA.

To evaluate the age, we first need to remember the effects of metallicity in stellar evolution. For such masses, increasing Z turns into a decrease of the total luminosity and effective temperature at each given evolution stage, as well as a slower evolution time-scale. Such features can also be rendered by de-

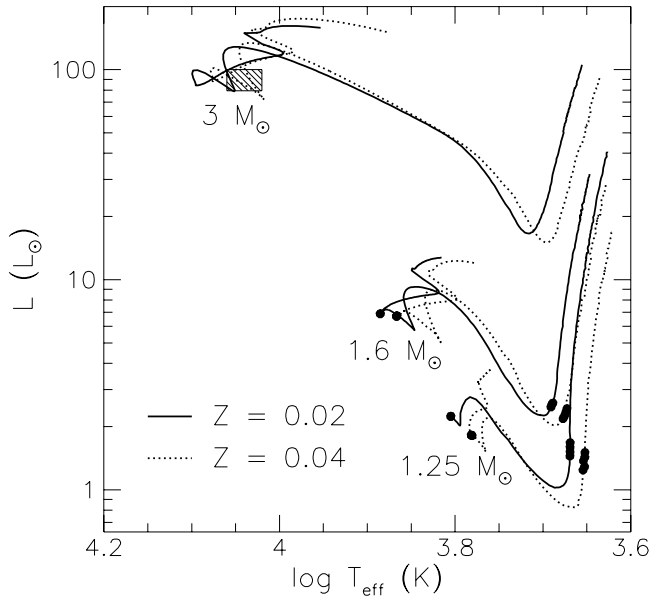


Fig. 2. Hertzsprung-Russell diagram showing the predicted positions of the second and third components of TY CrA, depending on the assumed age for the first component (see text). Obviously, the PMS positions correspond to t_{PMS} while at t_{MS} , both stars are located on their respective ZAMS

creasing the total mass at constant Z : total mass and metallicity conspire to the same changes concerning HRD location and age. This metallicity effect is well illustrated in the case of TY CrA. Indeed, Fig. 1 clearly indicates that if TY CrA is of solar metallicity, its corresponding track hardly crosses the observational box, while if its metallicity is twice as much, its track bluntly crosses the box. We also note that the age determination is even more intricate as the tracks penetrates the box two times (whatever Z), one before the zero-age main sequence (ZAMS; see the fill dots) is reached and another during the main sequence. This inevitably leads to two very different age predictions for the TY CrA system: one very small ($t_{\text{PMS}} \simeq 3 \cdot 10^6$ yr or $3.5 \cdot 10^6$ yr for $Z = 0.02$ or 0.04), and another considerably larger ($t_{\text{MS}} \simeq 1.5 \cdot 10^8$ yr or $\simeq 10^8$ yr for the same Z , respectively). We however observe that if $Z \simeq 0.02$, t_{MS} is only marginally possible. Note also that t_{PMS} is compatible with the predictions of Bibo et al. (1992).

Let us finally emphasize that both the secondary and tertiary components have very different internal structure depending on their age: at t_{PMS} , they are still partially convective and consequently less condensed than if they were mostly in radiative equilibrium like at t_{MS} .

Figure 2 shows the corresponding HRD locations of the second and third TY CrA components by assuming t_{PMS} or t_{MS} . Table 2 summarizes the stellar evolution predictions concerning the surfaces of the second and third components.

Table 2. Summary of the stellar evolution predictions concerning the TY CrA system

TY CrA component	t_{PMS}^a			t_{MS}^b		
	L (L_{\odot})	T_{eff} (K)	R (R_{\odot})	L (L_{\odot})	T_{eff} (K)	R (R_{\odot})
Second ($Z = 0.02$)	2.6	4880	2.3	6.9	7680	1.5
Third ($Z = 0.02$)	1.6	4670	1.9	2.2	6380	1.2
Second ($Z = 0.04$)	2.3	4720	2.3	6.7	7350	1.6
Third ($Z = 0.04$)	1.5	4510	2.0	1.8	6040	1.2

^a $t_{\text{PMS}} = 3.0 \cdot 10^6$ yr for $Z = 0.02$; $t_{\text{PMS}} = 3.5 \cdot 10^6$ yr for $Z = 0.04$

^b $t_{\text{MS}} = 1.5 \cdot 10^8$ yr for $Z = 0.02$; $t_{\text{MS}} = 1.0 \cdot 10^8$ yr for $Z = 0.04$

3. Three body dynamics

Although several non-planar triple stellar systems have been identified, it appears interesting to investigate the dynamics of such an unusual stellar system. Due to three body motion, the two considered orbits (binary system and tertiary) interact and may evolve slowly. In particular, the today eclipsing binary might not remain eclipsing permanently, thanks to the evolution of its orbital plane. Also the question of the stability of such a system might be addressed. Finally, this could give clues for understanding the still puzzling problem of the non-synchronism of the binary.

The interaction between the three components of the TY CrA system can be separated into two classes: three body interactions and tidal effects, mainly arising between the two components of the close binary. We will see below that tidal effects have a crucial role for ensuring the stability of the system. However, to make this appear clearly, we develop in this section a purely three body model, ignoring thus tidal effect which will be reintroduced afterwards.

3.1. Basic equations of motion

Referring the positions of the three components of the system with respect to the center of mass of the whole system by the radius vectors \mathbf{r}_i , $i = 1, 2, 3$, we start with the classical Newton equations

$$\frac{d^2 \mathbf{r}_i}{dt^2} = \mathcal{G} \sum_{j=1,2,3, j \neq i} m_j \frac{\mathbf{r}_j - \mathbf{r}_i}{|\mathbf{r}_j - \mathbf{r}_i|^3} \quad (1)$$

where \mathcal{G} is the gravitational constant. We reduce the order of the system introducing the relative positions of i) the secondary with respect to the primary; ii) the tertiary with respect to the center of mass of the binary system:

$$\mathbf{r} = \mathbf{r}_2 - \mathbf{r}_1; \quad (2)$$

$$\mathbf{r}' = \mathbf{r}_3 - \mathbf{r}_c = \mathbf{r}_3 - \frac{m_1 \mathbf{r}_1 + m_2 \mathbf{r}_2}{m_1 + m_2}. \quad (3)$$

\mathbf{r} and \mathbf{r}' are in fact the classical Jacobi coordinates introduced to reduce the order of the N -body problem (see e.g. Laskar

1989). Another interest of \mathbf{r} and \mathbf{r}' is that their variations exactly describe the evolution of the two orbits we considered. Note that hereafter, all primed quantities will refer to the orbit of the tertiary, while corresponding non-primed quantities will refer to the orbit of the close binary. We may now introduce the following notations:

$$M = m_1 + m_2 + m_3; \quad (4)$$

$$\mu = \frac{m_2}{m_1 + m_2}$$

$$\mu' = \frac{m_3}{m_1 + m_2 + m_3}$$

$$r_{ij} = |\mathbf{r}_j - \mathbf{r}_i|, \quad \text{for } (i, j) \in [1, 3]^2; \quad (7)$$

μ and μ' are the mass parameters of the corresponding orbits.

Given these notations, Eqs. (1) can be rewritten in terms of variations equations for \mathbf{r} and \mathbf{r}' as

$$\frac{1}{\mathcal{E}M} \frac{d^2 \mathbf{r}}{dt^2} = -\frac{1-\mu'}{r^3} \mathbf{r} + \mu' (\beta \mathbf{r}' - \gamma \mathbf{r}) \quad (8)$$

$$\frac{1}{\mathcal{E}M} \frac{d^2 \mathbf{r}'}{dt^2} = -\alpha \mathbf{r}' + \mu(1-\mu)\beta \mathbf{r}$$

where we have defined

$$\alpha = \frac{1-\mu}{r_{13}^3} + \frac{\mu}{r_{23}^3}, \quad \beta = \frac{1}{r_{23}^3} - \frac{1}{r_{13}^3}, \quad \gamma = \frac{1-\mu}{r_{23}^3} + \frac{\mu}{r_{13}^3}. \quad (9)$$

The potential energy U of this system is

$$\frac{U}{\mathcal{E}M^2} = -\frac{\mu(1-\mu)(1-\mu')^2}{r} - \frac{\mu\mu'(1-\mu')}{r_{23}} - \frac{\mu'(1-\mu)(1-\mu')}{r_{13}}. \quad (10)$$

The potential energy U_0 corresponding to the unperturbed orbits reads

$$\frac{U_0}{\mathcal{E}M^2} = -\frac{\mu(1-\mu)(1-\mu')^2}{r} - \frac{\mu'(1-\mu')}{r'}, \quad (11)$$

so that the perturbing potential $U_1 = U - U_0$ is

$$\frac{U_1}{\mathcal{E}M^2} = \mu'(1-\mu') \left[(1-\mu) \left(\frac{1}{r'} - \frac{1}{r_{13}} \right) + \mu \left(\frac{1}{r'} - \frac{1}{r_{23}} \right) \right]. \quad (12)$$

Adding U_1 to the Hamiltonian H_0 of the unperturbed system, we may now write the Hamiltonian H of the perturbed system:

$$\frac{H}{\mathcal{E}M^2} = -\frac{\mu(1-\mu)(1-\mu')^2}{2a} - \frac{\mu'(1-\mu')}{2a'} + \frac{U_1}{\mathcal{E}M^2}, \quad (13)$$

where a and a' are the semi-major axis of both orbits. For both orbits, we introduce now the classical conjugate Delaunay elements as

$$\begin{aligned} l; L &= \sqrt{(1-\mu)a\mathcal{E}M} \\ \omega; G &= \sqrt{(1-\mu)a\mathcal{E}M(1-e^2)} \\ \Omega; \Theta &= \sqrt{(1-\mu)a\mathcal{E}M(1-e^2)} \cos i \\ l'; L' &= \sqrt{a'\mathcal{E}M} \\ \omega'; G' &= \sqrt{a'\mathcal{E}M(1-e'^2)} \\ \Omega'; \Theta' &= \sqrt{a'\mathcal{E}M(1-e'^2)} \cos i' \end{aligned} \quad (14)$$

In these equations, l and l' are the mean anomalies in both orbits, while the other symbols have their usual meaning as orbital elements (semi-major axes, eccentricities, inclinations, longitudes of the nodes and argument of periastra). To avoid singularities for zero inclinations and eccentricities, it is convenient to replace the Delaunay elements by the Poincaré elements:

$$\lambda = l + \omega + \Omega \quad ; \quad \Lambda = L \quad (4)$$

$$\eta = -\sqrt{2(L-G)} \sin \varpi; \quad \xi = \sqrt{2(L-G)} \cos \varpi. \quad (15)$$

$$q = -\sqrt{2(G-\Theta)} \sin \Omega; \quad p = \sqrt{2(G-\Theta)} \cos \Omega$$

Here λ stands for the mean longitude and $\varpi = \omega + \Omega$ is the longitude of periastron. Of course, similar definitions are introduced for the orbit of the tertiary. The equations of motion become now

$$\begin{aligned} \frac{d\lambda}{dt} &= \frac{1}{\rho} \frac{\partial H}{\partial \Lambda} & \frac{d\eta}{dt} &= \frac{1}{\rho} \frac{\partial H}{\partial \xi} & \frac{dq}{dt} &= \frac{1}{\rho} \frac{\partial H}{\partial p} \\ \frac{d\Lambda}{dt} &= -\frac{1}{\rho} \frac{\partial H}{\partial \lambda} & \frac{d\xi}{dt} &= -\frac{1}{\rho} \frac{\partial H}{\partial \eta} & \frac{dp}{dt} &= -\frac{1}{\rho} \frac{\partial H}{\partial q} \\ \frac{d\lambda'}{dt} &= \frac{1}{\rho'} \frac{\partial H}{\partial \Lambda'} & \frac{d\eta'}{dt} &= \frac{1}{\rho'} \frac{\partial H}{\partial \xi'} & \frac{dq'}{dt} &= \frac{1}{\rho'} \frac{\partial H}{\partial p'} \\ \frac{d\Lambda'}{dt} &= -\frac{1}{\rho'} \frac{\partial H}{\partial \lambda'} & \frac{d\xi'}{dt} &= -\frac{1}{\rho'} \frac{\partial H}{\partial \eta'} & \frac{dp'}{dt} &= -\frac{1}{\rho'} \frac{\partial H}{\partial q'} \end{aligned} \quad (16)$$

where $\rho = M\mu(1-\mu)(1-\mu')$ and $\rho' = M\mu'(1-\mu')$ are the reduced masses corresponding to both orbital motions. These equations are equivalent to Eqs. (8). The system has 6 degrees of freedom.

3.2. The averaged problem

In order to study the secular evolution of the system, it is convenient to average Eqs. (16) over the short periods, namely the orbital motions. We see from Table 1 that all solutions lead to an orbital period for the tertiary larger than 100 days, which is much larger than the orbital period of the close binary (2.889 days; Kardopolov et al. 1981). We may thus claim that there is no obvious mean-motion resonance between both orbital motions; λ and λ' are independent variables and all the possible relative configurations between them are equiprobable. The averaging may then safely be done separately over these variables. We replace in Eqs. (16) the exact Hamiltonian H [Eq. (13)] by an averaged one \bar{H} defined as follows:

$$\bar{H} = \frac{1}{4\pi^2} \int_0^{2\pi} \int_0^{2\pi} H(\lambda, \lambda') d\lambda d\lambda'. \quad (17)$$

As the averaged Hamiltonian does not depend on λ and λ' , it is obvious from Eqs. (16) that the semi-major axes a and a' remain secularly constant, which is a classical result for non-resonant orbits. The averaged problem has therefore only 4 degrees of freedom.

It is possible to reduce once more the order of the system using the conservation of the total angular momentum of the whole system. To do so, we consider as usual a “natural” referential

frame ($OXYZ$) of the system where the angular momentum C is assumed parallel to (OZ). In the following, we will refer this referential frame as the natural one, while the original one will be referred as the “sky referential frame”. Measuring the angular orbital elements with respect to that referential frame, it is well known (Laskar 1989) that $\Omega - \Omega' = \pi$. We also have obviously

$$\rho G \cos i + \rho' G \cos i' = C; \quad (18)$$

$$\rho G \sin i - \rho' G \sin i' = 0, \quad (19)$$

where C is the constant angular momentum. This allows to directly express Θ and Θ' as a function of G , G' and C . The system reduces then to 2 degrees of freedom with (η, ξ, η', ξ') as dependent variables, to which the additional equation $d\Omega/dt = \partial H/\partial C$ must be added.

3.3. The numerical study

In order to investigate the dynamics of this triple system, we carried out a numerical integration of the averaged system over 50 000 years, taking as input the different solutions from Table 1. For the orbit of the close binary, we took the orbital elements given in Paper II. However, as it is not possible to constrain the longitude of the nodes (Ω and Ω') for both orbits, these parameters remained free. It is nevertheless obvious from rotational invariance that the Hamiltonian is only a function of $\Omega - \Omega'$. We thus tried different integrations taking various initial values for $\Omega - \Omega'$.

Once the initial conditions are fixed, the angular momentum of the system is computed, and the problem is translated into the natural reference frame, where the 2 degrees of freedom problem is numerically integrated. This requires the evaluation of the averaged Hamiltonian \bar{H} and of its derivatives with respect to the four dependent variables and C at each step. As reported below, the eccentricity of the close binary appears to vary from 0 to 1. Our description of secular dynamics must then be correct for any value of eccentricity. Hence, we cannot use here the classical expansions of \bar{H} in powers of e , typical of Celestial Mechanics. The averaging integral is numerically performed with a classical Gaussian quadrature rule using a 70×70 points grid. The averaged equations of motion are then numerically integrated using a 4th order Runge-Kutta scheme with adaptive step-size control. This procedure is identical to that of the Extended Schubart Integrator, used to compute the motion of Solar-System asteroids trapped in mean-motion resonances with Jupiter, as described in Moons (1993; 1994).

A general trend is that all solutions from Table 1 and all initial values for $\Omega - \Omega'$ give similar results, i.e., they reveal a similar behavior. Figures 3–6 show the temporal evolution of the most important orbital parameters for initial conditions ($t = 0$) corresponding to solution #1 from Table 1 and $\Omega - \Omega' = 100^\circ$. The first obvious conclusion is that the orbit of the binary is much more affected by perturbations than that of the tertiary. Surprisingly, the binary orbit appears to become regularly highly eccentric (Fig. 3), while its inclination (with respect to the natural referential frame) drops sharply by more than 40° at the same

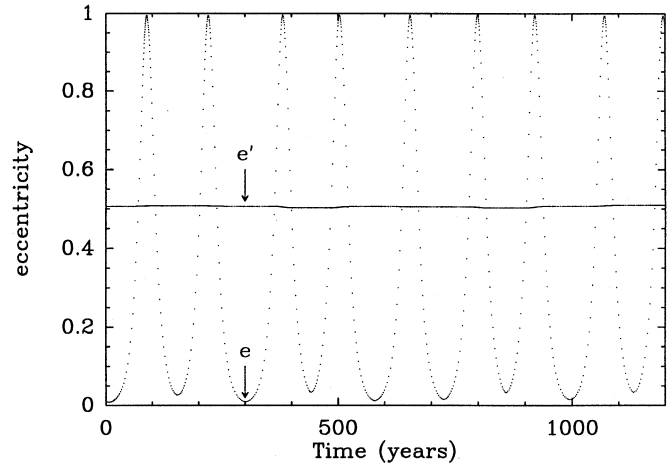


Fig. 3. Evolution of the eccentricities of the close binary (e) and the tertiary orbit (e') as a function of time for 1 200 years under the effects of pure 3-body dynamics. A quasi-periodic behavior (confirmed by integration over a longer time scale) is clearly detected; the close binary becomes very eccentric every ~ 150 years. Conversely, the eccentricity of the tertiary orbit is very stable. Only very small variations are recorded

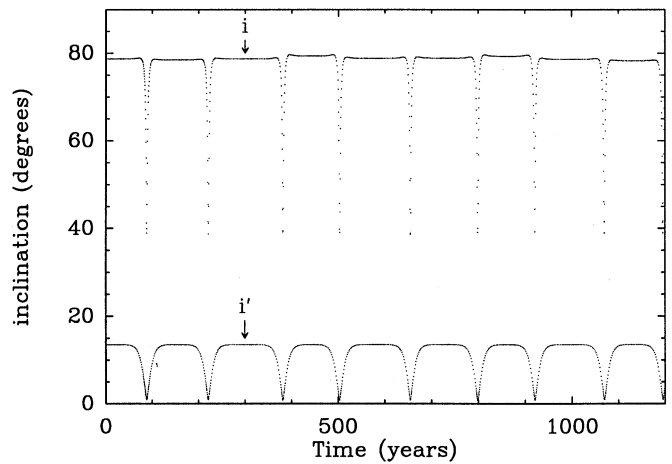


Fig. 4. Evolution of the inclinations of the close binary (i) and the tertiary orbit (i') with respect to the natural referential frame as a function of time, in the same conditions as in Fig. 3. Both inclinations appears to remain roughly constant most of the time, but drop regularly. These sudden variations correspond to the peak values for the eccentricity e . The variations of i' are much less important than for i'

time the eccentricity becomes large (Fig. 4). The orbit naturally precesses simultaneously, showing thus that the orbital plane of the binary orbit is far from being stable. Conversely, the orbit of the tertiary appears much more stable. Its eccentricity is almost constant (Fig. 3). Its inclination (always with respect to the natural referential frame) also presents a similar behavior to that the binary orbit, but the amplitude of the variations is here far less (Fig. 4); indeed, i' always remain between 0° and 13° , showing that the orbital plane of the tertiary remains roughly constant, almost perpendicular to the global angular momentum, while

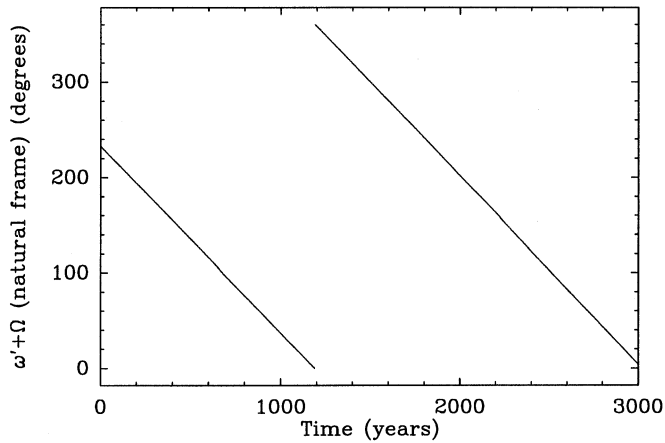


Fig. 5. Evolution of the longitude of perihelion $\varpi' = \Omega' + \omega'$ of the tertiary orbit with respect to the natural referential frame as a function of time. The orbit precesses within ~ 1800 years

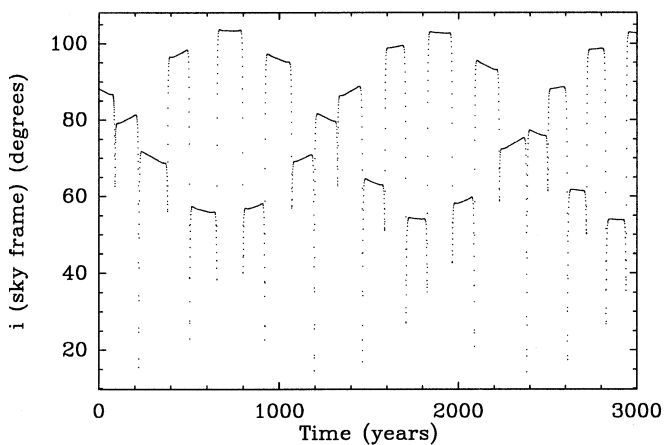


Fig. 6. Evolution of the inclination i of the close binary with respect to the sky referential frame as a function of time. Due to the combination with orbit precession, a more complex behavior than in Fig. 4 is recorded

the orbit regularly precesses over a longer time-scale, as illustrated in Fig. 5. These results were independently confirmed by a numerical integration of Eqs. (8).

Of course, once back in the sky referential frame, the behavior of the angular orbital elements is more complex, due to the combination of precession and nutation of the orbits. This is illustrated in Fig. 6, where the variations of the binary inclination i with respect to that frame are reported. The resulting behavior is more complex than in Fig. 4. This illustrates the advantage of performing all calculations in the natural referential frame. However, the important variations reported on Fig. 6 show that within that simple model, the today eclipsing binary is not expected to remain eclipsing permanently, since this would require an inclination permanently close to 90° .

The general behavior described here was recorded for all input solutions taken from Table 1, and for all values of $\Omega - \Omega'$. Varying $\Omega - \Omega'$ changes almost nothing to the results. It only

shifts the orbital precessing motion by a given constant angle. The different solutions from Table 1 reveal all the same quasi-periodic behavior, with only small changes to the period of that behavior. In particular (this is in fact the most important effect), for solutions #4 and #5, the period of the quasi-periodic motion of the eccentricities and the inclinations is roughly divided by a factor 2. This may be understood by the fact that for these solutions, the orbital period of the tertiary is roughly half of that for the first three solutions.

3.4. Interpretation

The recorded dynamical behavior may be understood when comparing the angular momenta of the orbits. The two angular momenta are ρG and $\rho' G'$, where G and G' are defined in Eqs. (14). It is worth noticing that the angular momentum of the tertiary orbit is significantly larger than that of the orbit of the binary. Considering the input data of solution #1 from Table 1, we found $\rho' G' / \rho G \simeq 4.79$. This is enough to consider that the total angular momentum of the system is mainly due to the tertiary orbit, since the tilt angle between its angular momentum and the global one cannot exceed $\arcsin(1/4.79) \simeq 12^\circ$.

Moreover, as the semi-major axes are constant, and that keplerian angular momenta are proportional to $\sqrt{a(1-e^2)}$, we see obviously that the angular momentum of the binary orbit will remain small compared to the global one C . Therefore, the angular momentum of the tertiary is forced to remain permanently close to C , showing that i) the eccentricity of the tertiary should not vary drastically ii) its orbital plane should remain close to the (OXY) plan of the natural referential frame, i.e., roughly perpendicular to C . This is obviously confirmed by the numerical integration.

Conversely, the orbit of the binary is expected to be the subject of more drastic changes. The behavior reported above may be described in the frame of the *Kozai mechanism* (Kozai 1962). This mechanism applies in the Solar System for comets with originally highly inclined orbits with respect of the ecliptic. Under the effect of secular planetary perturbations (mainly arising from Jupiter), the orbit evolves, but the rotational invariance of the averaged problem shows that the z -component of the orbital angular momentum of the comet, i.e., $J_z = \sqrt{a(1-e^2)} \cos i$ should remain constant. Therefore, an orbit initially highly inclined and weakly eccentric may become weakly inclined but highly eccentric to keep J_z constant. This occurs indeed periodically with the precession of the argument of perihelion ω . As pointed out by Bailey et al. (1992), this mechanism is responsible for the origin of most sun-grazer comets in our Solar System, in particular those of the Kreutz group. Within that mechanism, the temporal evolution of both inclination and eccentricity is similar to what is obtained on Figs. 3 and 4.

A similar mechanism is at work here on the orbit of the binary. Since the orbit of the tertiary is close to the (OXY) plane, we see that the longitude of its node Ω' is not well defined. This means precisely that the Hamiltonian H is expected to depend only weakly on Ω' ; $\partial H / \partial \Omega'$ is then small. By rotational invariance, the Hamiltonian is only a function of $\Omega - \Omega'$, showing

that $\partial H/\partial \Omega$ is also small. Thanks to Eqs. (16), we thus see that Θ should be roughly constant. This is exactly the context of the Kozai mechanism: any sharp decrease of inclination should be accompanied by a increase of eccentricity. We saw that this is expected to occur periodically. Naturally, a similar mechanism is expected to apply for the tertiary orbit, but thanks to a larger angular momentum, its amplitude is far less than in the case of the binary orbit (Fig. 4).

In order to have a more quantitative point of view, let us focus on a first order expansion of the 3-body Hamiltonian (13). Contrary to usual habits in Celestial Mechanics, we will not expand it here in powers of e or e' , since these quantities might not remain small. However, as the semi-major axes do not evolve, we may stress that r/r' is small, and both r_{13} and r_{23} (hence H) might be expanded in ascending powers of r/r' (Legendre polynomials). To lowest non-zero order, we get

$$\frac{U_1}{\mathcal{E}M^2} = \frac{\mu(1-\mu)\mu'(1-\mu')}{2r'} \left[\frac{r^2}{r'^2} - 3 \frac{(\mathbf{r} \cdot \mathbf{r}')^2}{r'^4} + O\left(\frac{r^3}{r'^3}\right) \right]. \quad (20)$$

This expression may then be averaged over both orbital motions like in Eq. (17). After some algebra, we get

$$\begin{aligned} \frac{\bar{U}_1}{\mathcal{E}M^2} = & -\frac{1}{8(1-e^2)^{3/2}} \frac{a^2}{a'^3} \mu(1-\mu)\mu'(1-\mu') \times \\ & \{ [15(1-2x_2^2-x_1^2)\cos^2\omega + 30x_2x_3\sin\omega\cos\omega + \\ & 15x_2^2+12x_1^2-9] e^2 - 1 + 3x_1^2 \} + \frac{1}{a'} O\left(\frac{a^3}{a'^3}\right) \end{aligned} \quad (21)$$

where

$$\begin{cases} x_1 = \cos i \cos i' + \sin i \sin i' \cos(\Omega - \Omega') \\ x_2 = \sin i' \sin(\Omega - \Omega') \\ x_3 = \cos i' \sin i - \cos i \sin i' \cos(\Omega - \Omega') \end{cases}. \quad (22)$$

Higher order expansions are more complex, but they may be obtained straightforwardly. First, it is interesting to note that ω' does not appear in Eq. (21). Hence, according to Eqs. (14), the variations of e' are only higher order. This illustrates why e' remains almost constant in any case. If we assume now $\Omega - \Omega' = \pi$, we also get to lowest order

$$\frac{d\Theta}{dt} = \frac{1}{\rho} \frac{\partial U_1}{\partial \Omega} = -\frac{15\mu\mathcal{E}Me^2}{16(1-e^2)^{3/2}} \frac{a^2}{a'^3} \sin 2i \sin 2\omega \sin i' + \frac{1}{a'} O\left(\frac{a^3}{a'^3}\right). \quad (23)$$

As i' remains small (for angular momentum conservation purpose), we see that this quantity remains also small, meaning that, as expected, Θ is roughly constant.

4. Tidal effects

4.1. The need for considering tidal effects

The three body calculations presented in the previous section did not take into account any tidal effect between the individual

stars constituting the TY CrA system. However, taking them into account cannot be avoided. First, it is well known that the dynamics of short period binaries is substantially affected by mutual tidal effects. In particular, binaries with orbital periods less than a cut-off period are expected to be circularized that way. From statistical observations, this cut-off periods is estimated to ~ 8 days (Koch and Hvrinak 1981), although observations of peculiar clusters gave smaller (5.7 days; Mayor and Mermilliod 1984) or larger values (10 – 11 days; Mathieu & Mazeh 1988). In any case, the orbital period of the close binary of the TY CrA system is far less than the cut-off value, showing that tidal effects within that binary are to be considered. Conversely, we may assume safely that tidal effects are limited to the binary only, i.e., that tidal effects involving the third component may be neglected.

Independently from this, Fig. 3 shows obviously that the three-body model of the previous section cannot be satisfactory: the eccentricity of the binary is expected to sometimes almost reach 1 (the exact peak value obtained in the numerical integrations was about 0.995). Remembering that the semi-major axis is constant, one sees that the periastron distance between the two primaries must become very small whenever the eccentricity is high. The semi-major axis of the binary is estimated to $13.9 R_\odot$ (Paper II) at present-time zero eccentricity; the periastron is then expected to be as small as $0.0695 R_\odot$ for $e = 0.995$. This is far less than the radius of both stars at any age (see Table 2), showing that the binary should in fact have already collapsed into a single star unless tidal effects prevent the orbit from evolving to high eccentricity values. This illustrates the need for considering tidal effects.

4.2. Various tidal mechanism

Several mechanisms generate tidal effects in close binaries. They all tend to synchronize the rotation of both components and the orbital motion and to circularize the orbit. In the case when the rotation axis would not be perpendicular to the orbital plane, the tidal effects also act to align both orbital and rotational angular momenta. Indeed, for an isolated close binary, it was shown (Hut 1980) that the only possible equilibrium state is characterized by i) alignment of the angular momenta, ii) circularity, and iii) corotation, irrespective to any tidal mechanism. The efficiency of the different mechanism may be compared evaluating characteristic circularization (t_{circ}) and synchronization (t_{sync}) times for each of them. Basically, for a given tidal mechanism making the eccentricity and the rotation velocities N of both stars vary, one may define these times as (Zahn 1977)

$$\frac{1}{t_{\text{circ}}} = -\frac{1}{e} \frac{de}{dt}; \quad (24)$$

$$\frac{1}{t_{\text{sync}}} = -\frac{1}{N-n} \frac{dN}{dt}, \quad (25)$$

where n is the mean angular orbital velocity. One t_{sync} can of course be defined for each star (one for each N_i), while for t_{circ} , the contribution of both stars must be added.

The first mechanism invoked is the *equilibrium tide*: due to tidal attraction from its companion, each component is distorted from a spherical or axisymmetric shape and reaches an equilibrium figure. The tide resulting from this interaction may be separated into two distinct effects, which were analyzed by Alexander (1973) and Kopal (1978):

1. an effect arising from the rotation of each component on itself, independent from any mutual interaction. This effect vanishes when the rotation axes are perpendicular to the orbital plane, otherwise it only acts on the angular orbital elements, and does not affect a and e . This effect may be called *rotational effect*. It does not contribute to circularization nor synchronization, but to precession and nutation of the rotation axis. Its efficiency may be estimated by a characteristic time t_{rot} for each component # i defined by Alexander (1973):

$$(t_{\text{rot}})_i = \frac{\mathcal{G} M_i a^2}{N_i^2 (k_2)_i R_i^5} \frac{2\pi}{n}, \quad (26)$$

where R_i stands for the radius of the corresponding component, and $(k_j)_i$, $j = 2, 3 \dots$ for dimensionless constants related to the internal structure of that component, known as apsidal constants.

2. a “lagging-tide” effect, due to the viscosity of the material constituting each component. Consequently, the tidal bulge raised by one component onto its companion cannot perfectly points towards the companion, but lags by a given angular amount referred as tidal lag. The analysis of the secular action of this effect on the orbital elements of the binary was achieved by Alexander (1973), Kopal (1978) and Hut (1981; 1982), in the so-called weak-friction case, where the tidal lag is assumed proportional to the relative angular velocity $N_i - n$ (this is true for small enough lags). Alexander computed the characteristic times t_{circ} and t_{sync} for that effect as (here given for component #1)

$$(t_{\text{circ}})_1 = \frac{m_1}{m_2} (1 - e^2)^5 \left(\frac{a}{R_1} \right)^5 \frac{1}{T_1 N_1 (k_2)_1} \frac{2\pi}{n}; \quad (27)$$

$$(t_{\text{sync}})_1 = \frac{m_1}{m_2} \left(1 + \frac{m_1}{m_2} \right) (1 - e^2)^{9/2} \times \left(\frac{a}{R_1} \right)^3 \frac{2\pi g_1^2}{T_1 n^2 (k_2)_1}, \quad (28)$$

where g_1 is the gyration radius of component #1 defining its moment of inertia as $g_1^2 m_1 R_1^2$, and T_1 is a (small) constant delay time characterizing the lagging tide effect. T_1 is related to the mean viscosity of the star $\bar{\mu}$ by

$$\bar{\mu} = \frac{125}{242\pi} \frac{\mathcal{G} m_1^2}{R_1^4} (k_2)_1 T_1. \quad (29)$$

Evaluating $\bar{\mu}$ is not easy, but Press et al. (1975) showed that turbulent viscosity in radiative envelopes should dominate microscopic viscosity, giving thus an estimate for $\bar{\mu}$, t_{circ} and t_{sync} .

Another tidal mechanism inducing synchronization and circularization known as *dynamical tides* was analyzed by Zahn

(1975; 1977). This occurs when the non-adiabatic oscillations driven on one component by the perturbing action of its companion are damped by radiative dissipation. This leads to a torque applied to the star, thus coupling orbital motion and rotation. Zahn (1977) showed that this effect dominates when a radiative envelope is present, thus for early-type stars, which may be the case at least for the $3.0 M_\odot$ primary in TY CrA. Zahn (1977) gave the characteristic times t_{sync} and t_{circ} for that effect:

$$\frac{1}{(t_{\text{sync}})_1} = 52^{2/3} \sqrt{\frac{G m_1}{R_1^3} \frac{m_2^2}{m_1^2}} \left(1 + \frac{m_2}{m_1} \right)^{5/6} \frac{(E_2)_1}{g_1^2} \left(\frac{R_1}{a} \right)^{17/2}; \quad (30)$$

$$\frac{1}{(t_{\text{circ}})_1} = \frac{21}{2} \sqrt{\frac{G m_1}{R_1^3} \frac{m_2}{m_1}} \left(1 + \frac{m_2}{m_1} \right)^{11/6} (E_2)_1 \left(\frac{R_1}{a} \right)^{21/2}, \quad (31)$$

(for component #1) where $(E_j)_i$, $j = 2, 3 \dots$ are dimensionless constants characterizing the dynamical tide, analogous to the apsidal constants $(k_j)_i$ for equilibrium tides.

A final mechanism was discovered by Tassoul & Tassoul (1992, and Refs. therein). They showed that tidally driven meridional currents within each component act for circularization and synchronization. They also gave characteristic times:

$$(t_{\text{sync}})_1 (\text{yr}) = \frac{14.4 \times 10^{-N/4} m_2}{m_1 (1 + m_2/m_1)^{3/8}} \times \left(\frac{L_\odot}{L_1} \right)^{1/4} \left(\frac{M_\odot}{m_1} \right)^{1/8} \left(\frac{R}{R_\odot} \right)^{9/8} \left(\frac{a}{R_1} \right)^{33/8}; \quad (32)$$

$$(t_{\text{circ}})_1 (\text{yr}) = \frac{14.4 \times 10^{-N/4}}{g_1^2 (1 + m_2/m_1)^{11/8}} \times \left(\frac{L_\odot}{L_1} \right)^{1/4} \left(\frac{M_\odot}{m_1} \right)^{1/8} \left(\frac{R}{R_\odot} \right)^{9/8} \left(\frac{a}{R_1} \right)^{49/8}, \quad (33)$$

where L_1 stands for the luminosity, and N is a characteristic exponent which may be taken equal to 0 for stars having radiative envelopes and to 10 for those having a convective envelope.

4.3. Application to TY CrA

Comparing the efficiency of the different tidal mechanism described above means evaluating and comparing the values of the corresponding characteristic times. One needs thus values for the various constants appearing in these expressions, once applied to the peculiar case of the close binary of the TY CrA system. Among them we first have the apsidal constants $(k_j)_i$. The complete treatment of the equilibrium tide only requires them up to $j = 4$ (Alexander 1973). It is well known (Kopal 1978) that these constants are defined by

$$(k_j)_i = \frac{j+1 - \eta_j(R_1)}{2j + 2\eta_j(R_1)}, \quad (34)$$

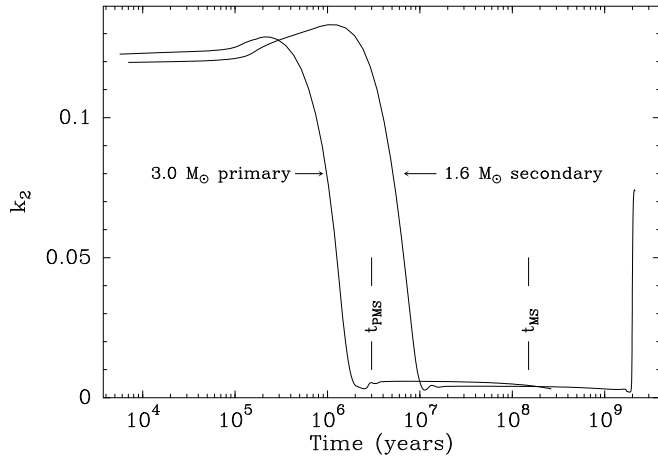


Fig. 7. Evolution of the first apsidal constant k_2 as a function of time for the components of the TY CrA central binary, assuming solar metallicity. The temporal location of t_{MS} and t_{PMS} for solar metallicity is indicated

Table 3. Values of apsidal constants, radius and gyration radius obtained for the close binary of the TY CrA system using the models of Siess et al. (1996), and assuming solar metallicity

Parameter	Primary (t_{MS})	Secondary (t_{MS})	Primary (t_{PMS})	Secondary (t_{PMS})
Mass (M_{\odot})	3.0	1.6	3.0	1.6
Radius (R_{\odot})	2.54	1.48	2.38	2.21
Gyr. radius	0.224	0.205	0.218	0.433
k_2	$4.31 \cdot 10^{-3}$	$4.00 \cdot 10^{-3}$	$5.21 \cdot 10^{-3}$	0.118
k_3	$9.36 \cdot 10^{-4}$	$8.38 \cdot 10^{-4}$	$1.09 \cdot 10^{-3}$	$4.38 \cdot 10^{-2}$
k_4	$3.15 \cdot 10^{-4}$	$2.80 \cdot 10^{-4}$	$1.39 \cdot 10^{-4}$	$2.27 \cdot 10^{-2}$

where $\eta_j(R_1)$ is the surface value of a particular solution $\eta_j(r)$ of the Radau differential equation

$$r \frac{d\eta_j}{dr} + \eta_j (\eta_j - 1) + 6D(\eta_j + 1) = j(j + 1), \quad (35)$$

with the initial condition $\eta_j(0) = j - 2$. Here $D = \rho(r)/\bar{\rho}(r)$, where $\rho(r)$ is the density (inside the star) at radius r , while $\bar{\rho}(r)$ stands for the mean density inside the sphere of radius r .

Solving these equations requires a stellar model to tabulate the function D . Standard determinations of k_j 's are given by Brooker & Olle (1955) for polytropic models with various indexes. However, these values appeared not satisfactory to us, as the apsidal constants they obtained are significantly sensitive to the polytropic index assumed. Moreover, these constants may depend on the age of the TY CrA system.

We thus decided to tabulate these quantities over the lifetime of both components of the binary. More precisely, for each model at a given age, we integrated the Radau equation to determine the k_j 's.

The results of this determination is illustrated on Fig. (7), where the principal apsidal constant (k_2) is plotted as a function of time for both components (the other ones present very similar behaviors). Schematically, for each star, k_2 remains high as long

Table 4. Values of characteristic times for the different tidal mechanisms invoked

Mechanism ($t_{PMS} : 3 \cdot 10^6$ yr)	t_{circ} (yrs)	$(t_{sync})_1$ (yrs)	$(t_{sync})_2$ (yrs)
Equilibrium tide	$2.488 \cdot 10^{10}$	$1.458 \cdot 10^{11}$	$1.175 \cdot 10^8$
with turbulence (Press et al. 1975)			
Dynamical tide (Zahn 1977)	$2.488 \cdot 10^{10}$	$6.246 \cdot 10^7$	$5.246 \cdot 10^8$
Meridional circulation (Tassoul & Tassoul 1992)	$2.028 \cdot 10^6$	$2.765 \cdot 10^4$	$1.993 \cdot 10^4$
Rotational effect (Alexander 1973)	$(t_{rot})_1 = 6536$ yrs $(t_{rot})_2 = 220.3$ yrs		
Mechanism ($t_{MS} : 1.5 \cdot 10^8$ yr)	t_{circ} (yrs)	$(t_{sync})_1$ (yrs)	$(t_{sync})_2$ (yrs)
Equilibrium tide	$3.846 \cdot 10^{12}$	$1.219 \cdot 10^{10}$	$1.193 \cdot 10^{11}$
with turbulence (Press et al. 1975)			
Dynamical tide (Zahn 1977)	$1.134 \cdot 10^{10}$	$4.129 \cdot 10^7$	$1.926 \cdot 10^9$
Meridional circulation (Tassoul & Tassoul 1992)	$3.903 \cdot 10^6$	$2.001 \cdot 10^4$	$4.762 \cdot 10^4$
Rotational effect (Alexander 1973)	$(t_{rot})_1 = 5658$ yrs $(t_{rot})_2 = 4792$ yrs		

as the star is pre main-sequence, and drops as soon as a radiative (and more dense) core grows. The temporal position of the two possible ages t_{PMS} and t_{MS} mentioned above is indicated (for solar metallicity). We clearly see on the plot the difference between these two models. At t_{MS} , both stars are basically on the main sequence, while this is only the case for the $3.0 M_{\odot}$ primary at t_{PMS} . Consequently, k_2 is significantly larger for the $1.6 M_{\odot}$ secondary at t_{PMS} .

This result also holds for k_3 and k_4 . Indeed, these constants are always smaller than k_2 for both stars, but they present temporal evolutions identical to k_2 . Some peculiar values for t_{MS} and t_{PMS} (solar metallicity) are given in Table 3. Comparing to Brooker & Olle (1955), we see that for t_{MS} , our values roughly correspond to those for a polytropic index 3.5. Comparing both models shows that the results are almost the same for the primary, while the apsidal constants for the secondary are larger by at least one order of magnitude at t_{PMS} than at t_{MS} . This is not surprising, since at both ages, the primary is a main sequence star, while the secondary is a pre-main sequence star at t_{PMS} .

Given these results, we thus computed the various characteristic times for all the tidal effects, for both ages. For the dynamical tidal torque constants $(E_2)_i$, $i = 1, 2$, we took ZAMS values corresponding to both stellar masses from Zahn (1975): $(E_2)_1 = 4.72 \cdot 10^{-8}$ and $(E_2)_2 = 2.41 \cdot 10^{-9}$. The results of characteristic time determination are listed in Table 4. We may note that in any case, the most powerful effects are i) the rotational effect for equilibrium tide ii) the meridional circulation model by Tassoul & Tassoul (1992). Indeed, the other effects can be neglected in the present case, since their characteristic times are always larger than the assumed age of the TY CrA system. It is

also worth noticing than the tidal effects are much more efficient on the secondary at t_{PMS} than at t_{MS} , because of its pre-main sequence state at t_{PMS} .

5. Dynamics of the TY CrA system with tidal effects

In order to properly distinguish the effect of each tidal mechanism, we carried out a numerical integration of the TY CrA system dynamics, adding the tidal effects to the basic three-body model described above. Table 4 shows that the meridional circulation effect by Tassoul & Tassoul (1992) is by far the strongest one among the possible effects. The other ones may be neglected. However, the weak-friction model is the only one for which closed evolution formulas for the orbital elements are available and valid for any configuration (high eccentricity, non-coplanarity. . .). We thus decided to use these formulas given in Alexander (1973), but adjusting at every time the characteristic constants T_i ($i = 1, 2$) in such a way that the characteristic times ($t_{\text{sync}})_i$ ($i = 1, 2$) of the weak friction model defined in Eq. (28) remain equal to the corresponding ones for the meridional circulation model, defined in Eq. (32). This may be justified by the fact that the evolution equations given by Alexander (1973) are derived from an average over the instantaneous perturbation equations, and that the general form of these equations is independent from any tidal mechanism. It was also shown by Hut (1980) that for any tidally interacting binary, the only possible equilibrium is characterized by circularity, corotation and axes alignment, whatever the specific tidal mechanism; thus, only time-scales are important.

Since tidal effects work on coupling the orbital motion to the axial rotation of the stars, we must now compute the evolution of their rotation together with that of the orbital motion. We thus add now six new variables to the basic orbital elements, used to characterize the rotation of each component of the binary: the rotation velocities N_j ($j = 1, 2$), the ascending nodes ϕ_j ($j = 1, 2$) of the equatorial planes of the stars with respect to the natural referential frame, and the inclinations θ_j ($j = 1, 2$) of the rotation axes with respect to the OZ axis of the natural referential frame. Note that the synchronism of component # j with the orbital motion means exactly $N_j = n$, $\phi_j = \Omega$ and $\theta_j = i$. Note also that the orbital angular momentum of the whole system is no longer constant, due to the tidal interaction. In fact, one should consider the total angular momentum (orbital+rotational) of the system, and an appropriate referential frame. However, since in any case, the rotational angular momenta are much smaller than the orbital ones, we may consider that the total orbital angular momentum is roughly constant, and we will keep the natural referential frame introduced in Sect. 3. Nevertheless, as the orbital angular momentum is no longer exactly constant, the reduction of the order of the system to be integrated no longer holds. We are then back to the averaged version of Eqs. (16). Moreover, as tidal effects may cause the semi-major axes vary, we cannot consider them as constant as previously. Finally, the number of dependent variables is now 16, i.e., 10 orbital parameters and 6 “rotational” ones.

However, we keep the averaged formulation of the problem. Alexander (1973) and Kopal (1978) calculated the averaged form of the variational equations for all orbital elements and rotational parameters for the weak-friction model. The reader is referred to Eqs. (3.30)–(3.40), (4.21)–(4.23), and (4.32)–(4.34) from Alexander (1973), which are valid for any eccentricity.

If the binary was alone, there would be no reason for both rotation axes not to be perpendicular to the orbital plane. However, the presence of the tertiary component may change this simple picture. We indeed saw above that according to pure three-body motion, the orbital plane of the binary is expected to present periodic drastic changes over a typical time of a few hundreds years. Hence, if we want the orbital axes to remain perpendicular to that orbital plane, the tidal effects which act on coupling the rotation and the orbital motion need to be strong enough to make the rotation axes “follow” the secular evolution of the orbital plane. This is far from being obvious, and it is therefore legal to consider that the rotation axes might not be aligned. Moreover, as it is well known from $v \sin i$ measurements that if we assume that the rotation axes are perpendicular to the orbital plane, the binary of the TY CrA system surprisingly appears non-synchronous, it thus appears that there is no observational fact supporting this assumption. This conclusion was indeed reached by Casey et al. (1993).

We are therefore free of choosing any set of initial values in our simulation runs for the initial rotational parameters N_j , θ_j , ϕ_j , $j = 1, 2$. The only constraint on these parameters are the present values of $v \sin i$ measured towards both stars (8 km s^{-1} for the primary and 35 km s^{-1} for the secondary; Casey et al. 1993; Papers II and III), considering them as initial values.

For each age (t_{PMS} or t_{MS}), several runs with different initial conditions were carried out; they all revealed similar behaviors, showing that the dynamics depends only weakly on the initial conditions. However, significant differences appeared between the behavior recorded for the two models. We present now two typical runs, one for each age. In each run, the angles θ_j and ϕ_j are initially chosen randomly, and the initial values for the rotation velocities N_j are fixed to fit to the present values of the $v \sin i$'s.

Most of the runs revealed a very similar behavior which is reported below. However, in some cases, a significantly different one was detected, which is discussed afterwards.

5.1. The typical behavior

The dissipative tidal effects act on circularization, synchronization and alignment of the rotation axes with the orbital angular momentum within the close binary. However, such an equilibrium holds theoretically for an isolated binary. It is however worth noticing that a similar equilibrium may be reached for the 3-body TY CrA system. We first show results at t_{PMS} . Figure 8 shows the evolution of the semi-major axis a of the close binary. We see that after a smooth decrease, we reach a stable equilibrium value. Besides, the semi-major axis a' (not displayed here) of the tertiary remains unchanged, as tidal effect do not act on it.

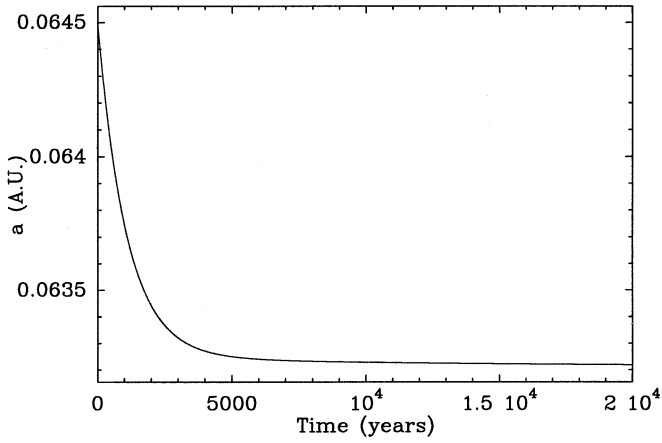


Fig. 8. Evolution of the semi-major axis a of the binary over 20 000 yrs under the effects of dissipative tidal effects, at t_{PMS} . An equilibrium value is reached within $\sim 6\,000$ yrs

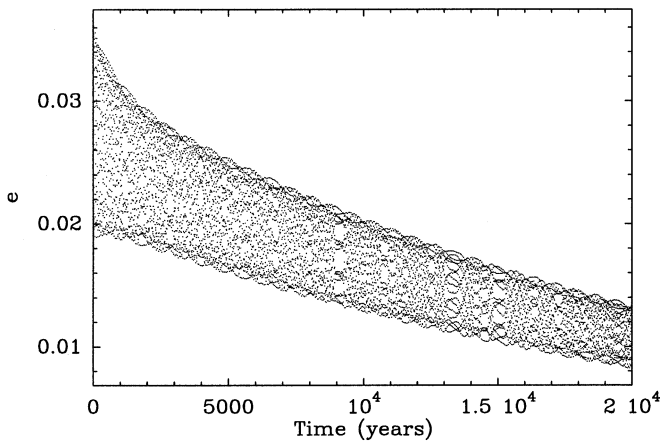


Fig. 9. Evolution of the eccentricity e of the orbit of the binary over 20 000 yrs under the effects of dissipative tidal effects, at t_{PMS} . We note a gradual circularization

Figure 9 shows the evolution of the eccentricity e of the binary. Contrary to Fig. 3, the eccentricity remains small; thanks to the tidal effects, no Kozai-like behavior is present. In fact, such a behavior still exists, but its amplitude remains small (between $e = 0.02$ and $e = 0.03$), and its period is much smaller than in Fig. 3. Reducing the amplitude of the Kozai mechanism just saves the binary from collapsing. The stability of the TY CrA system is actually ensured by tidal effects ! Concerning the evolution of the eccentricity of the tertiary e' (not displayed here), it is identical to that reported in Fig. 3.

We also note in Fig. 9 a gradual long-term circularization, which is clearly due to the dissipative effect.

Figure 10 shows the evolution of the inclinations of both orbits, relative to the natural referential frame. Compared to Fig. 4, we see that there is here no Kozai-like behavior anymore for the inclinations, which remains almost constant. Figure 11 shows the evolution of the longitude of the node Ω of the orbit of the binary. We note a precession over ~ 6000 yr.

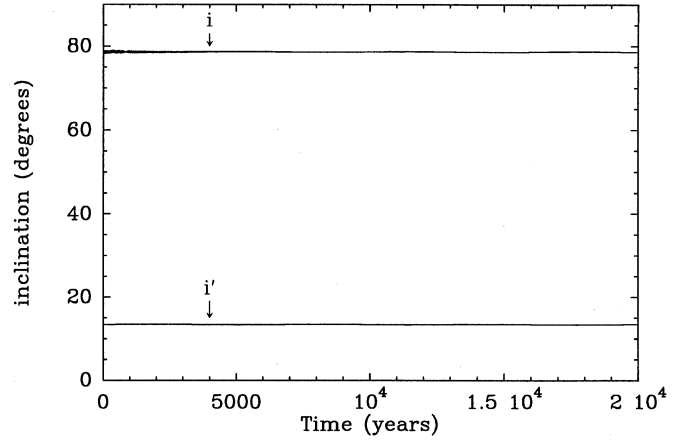


Fig. 10. Same as Fig. 9, but for the inclinations i and i' of both orbits, relative to the natural referential frame. There is no significant variation for i , while a small Kozai-like behavior is still present for i'

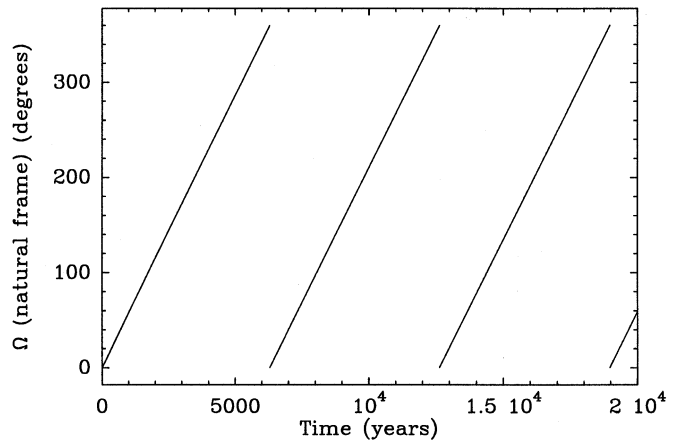


Fig. 11. Evolution of the longitude of the node Ω of the orbit of the binary as a function of time, in the same conditions as in Fig. 10. We note a precession over a period of 8000 years

Figure 12 illustrates the fact that the total orbital angular momentum almost remains constant: in the pure three-body model, the difference $\Omega - \Omega'$ (in the natural referential frame) is exactly 180° . Here, the variations of this quantity are reported, showing long-term but small amplitude oscillations around that value.

Figures 13 and 14 describe the evolution of the rotation of the components of the binary. Instead of showing the variations of the angles θ_i 's and ϕ_i 's ($i = 1, 2$), it is convenient here to display the evolution of the tilt angles ψ_i 's ($i = 1, 2$) between the rotation axes of each star and the orbital angular momentum of the binary. Note that ψ_i is defined by

$$\cos \psi_i = \cos \theta_i \cos i + \sin \theta_i \sin i \cos(\phi_i - \Omega) \quad i = 1, 2. \quad (36)$$

The variations of ψ_i 's ($i = 1, 2$) are displayed on Fig. 13. We see that the rotation axes quickly move to align with the orbital angular momentum of the binary.

Figure 14 shows the evolution of the rotation velocities of the stars, once divided by the mean orbital motion n (thus, 1

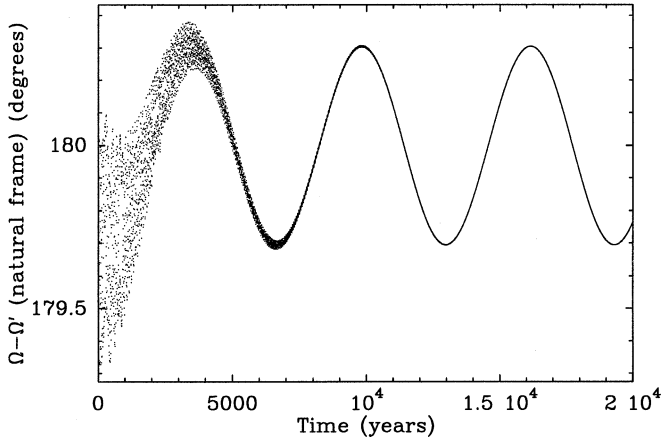


Fig. 12. Same as Fig. 11, but for the difference $\Omega - \Omega'$. It remains close to 180°

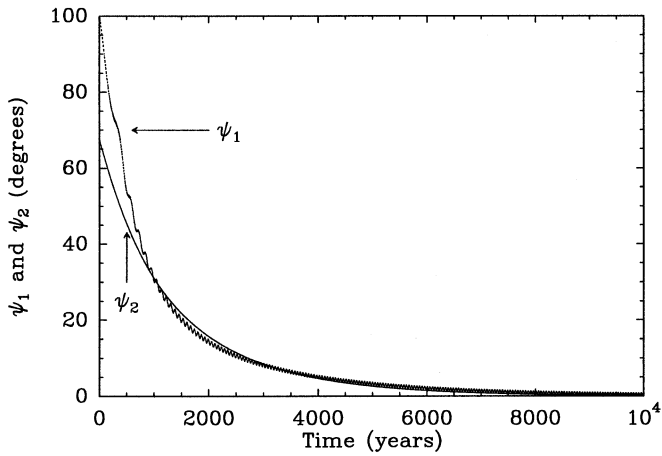


Fig. 13. Evolution of the tilt angles ψ_1 and ψ_2 characterizing the alignment of the rotation axes of the binary, under the effects of dissipative tidal effects, at t_{PMS} . We note a quick alignment process

means synchronism). The $3.0 M_\odot$ primary appears initially sub-synchronous. This is due to the assumed initial values of $v \sin i$'s. We see that both stars are synchronized within ~ 6000 yrs.

The behavior described here is characteristic for a tidally interacting binary. The binary approaches asymptotically an equilibrium characterized by corotation, coplanarity and circularization. Moreover, as expected (see Table 4), the synchronization is achieved earlier than the circularization. It was shown by Hut (1981) that this fact is valid for any binary for which the orbital angular momentum largely overcomes the rotational one. However, in the present case of TY CrA, there is a (philosophical) significant difference : due to the presence of the third companion, the orbital plane of the binary precesses while its inclination remains high. The angular momentum of the binary is therefore not constant, at least vectorially. However, it is a remarkable fact that this does not affect the equilibrium state of the binary. When the equilibrium is reached, the binary orbits like a “solid body” with the third component.

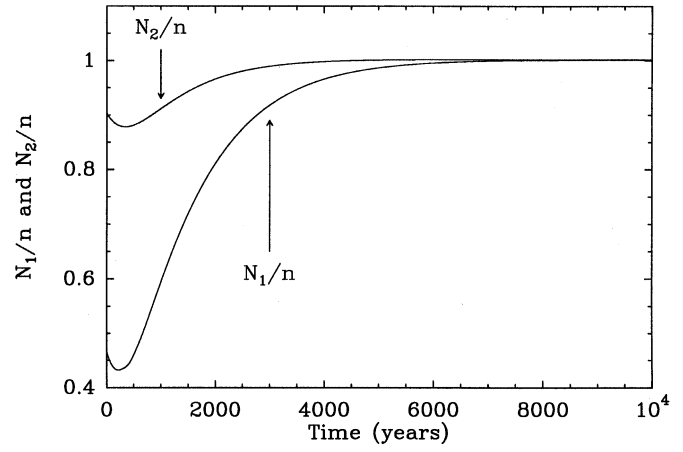


Fig. 14. Evolution of the rotation velocities of the binary components under the effects of dissipative tidal effects, at t_{PMS} . The rotation of the stars synchronizes with the orbital motion within ~ 6000 yrs

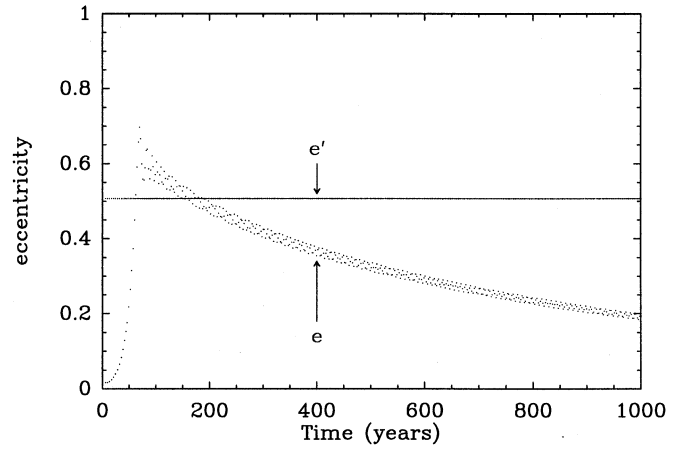


Fig. 15. Evolution of the eccentricities of both orbits under the effects of dissipative tidal effects, at t_{MS} . We note a gradual circularization of the binary following a strong increase of the eccentricity

We come now to present results of a similar run at t_{MS} . Compared to the run at t_{PMS} , we display here only those results which present significant differences.

Figures 15 and 16 show the temporal evolution of the eccentricity e of the binary, and of the tilt angles ψ_i 's ($i = 1, 2$). They must be compared to Figs. 9 and 13.

Here, the 3-body dynamics is strong enough to initiate a Kozai cycle (Fig. 15), with a strong increase of the eccentricity. Afterwards, the eccentricity slowly decreases to zero. The sudden increase of the eccentricity is accompanied by a very rapid synchronization and a quick alignment of the axes (Fig. 16), which take place much earlier than at t_{PMS} . This may be explained as follows: Thanks to smaller tidal coupling at t_{MS} (see Fig. 7 or Table 4), the 3-body dynamics is strong enough to initiate a full Kozai cycle, making the eccentricity of the binary increase without changing the semi-major axis. This causes the periastron distance between both components to decrease. But the tidal effects are stronger at periastron, when the distance be-

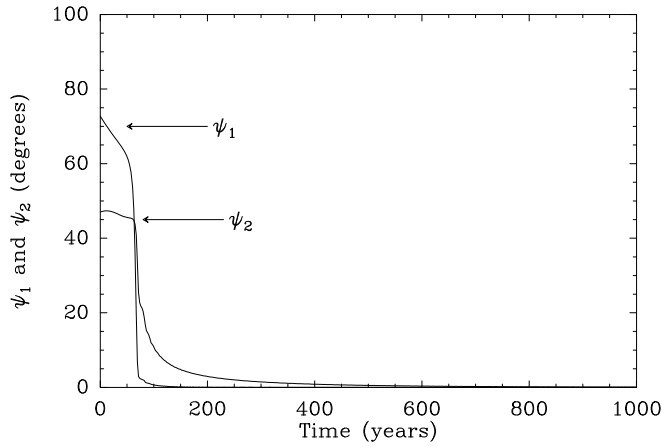


Fig. 16. Same as Fig. 13, but at t_{MS} . The alignment process is here much more rapid

tween the stars is smaller. Consequently, the Kozai cycle leads to a strong increase of the strength of the tidal effects, leading to a rapid synchronization of the binary. Finally, the equilibrium is reached more quickly than at t_{PMS} , thanks to the 3-body dynamics, and although the tidal effects are globally smaller (Table 4).

5.2. A peculiar behavior

Testing various initial configurations of the rotation axes reveals that the behavior described above is quite generic. In any case, the binary circularizes and synchronizes in a characteristic time-scale somewhat comparable to those for the meridional circulation model (Tassoul & Tassoul 1992) given in Table 4.

Considering the small values of these times, we would then expect the central binary to have already reached the equilibrium. From an observational point of view, this does not seem to be the case today (Paper II; Casey et al. 1993, 1995).

We come to describe now the results of a specific run which might give clues for understanding this peculiar problem. We first recall that in all our runs, once the orientation of the rotations axes (angles θ_i 's and ϕ_i 's) are chosen, the initial rotation velocities is fixed to fit the observed present $v \sin(i)$'s of the stars. In the following run, the initial orientation of the $3.0 M_{\odot}$ primary was nearly pole-on; thus, its initial rotation velocity was high (super-synchronous), contrary to all other possible orientations.

Figures 17–19 show the results of this run at t_{PMS} (the behavior of the eccentricity is not shown here, but it is similar to Fig. 9). We first note that the same equilibrium as previously is still reached, but somewhat later. The reason why the equilibrium is reached later may be seen from Fig. 18: the tilt angle ψ_1 of the $3.0 M_{\odot}$ primary appears to remain quite a long time close to 90° before dropping to zero. More precisely, this situation lasts as long as $N_1/n \gtrsim 0.4$, and disappears immediately afterwards.

It thus seems that a marginally stable equilibrium $\psi_1 = 90^{\circ}$ exists when the rotation of the primary is high enough. $\psi_1 = 90^{\circ}$

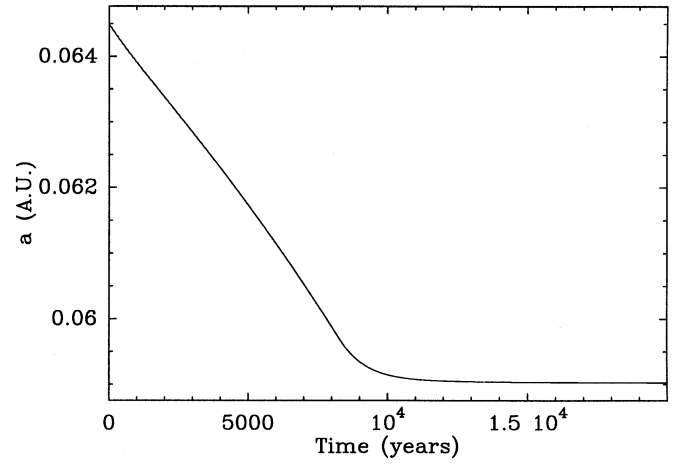


Fig. 17. Evolution of the semi-major axis a of the binary over 20 000 yrs under the effects of dissipative tidal effects, at t_{PMS} with an initially pole-on primary. An equilibrium value is reached within ~ 9 000 yrs

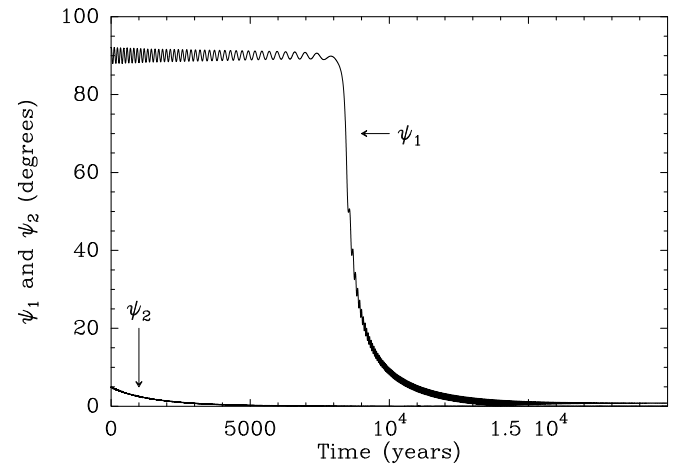


Fig. 18. Same as Fig. 17, but for the tilt angles ψ_1 and ψ_2 . The $3.0 M_{\odot}$ primary remains quite a long time at $\psi_1 = 90^{\circ}$, while the $1.6 M_{\odot}$ secondary is quickly aligned. This remains true even when the initial value of ψ_2 is high

means that the rotation axis of the $3.0 M_{\odot}$ primary lies in the orbital plane of the binary. As the binary is an eclipsing one, $\psi_1 = 90^{\circ}$ is compatible with a pole-on orientation of the rotation axis of the primary with respect to the line of sight. It must also be stressed that whenever ψ_1 remains around 90° , the rotation axis of the primary does not remain stable (both ϕ_1 and θ_1 evolve), but its evolution is constrained to the orbital plane of the primary.

Such a marginal equilibrium might apply for the today situation of the TY CrA system, and thus explain why the binary does not appear synchronized. Before concluding anything, we must examine the origin of this marginal equilibrium. First, we may note that it is not observed at t_{MS} . Figure 20 shows the evolution of the tilt angles ψ_1 and ψ_2 under the same initial condition as in Fig. 18, but at t_{MS} . We see that these angles drop to zero much more quickly than at t_{PMS} . Here again, the 3-body dynam-

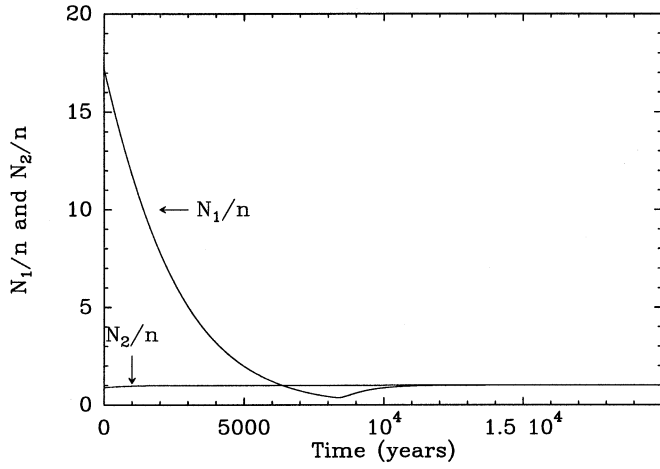


Fig. 19. Same as Fig. 17, but for the rotation velocities of the binary components. We see that the $3.0 M_{\odot}$ primary is initially highly super-synchronous, despite a very low $v \sin(i)$. This is due to the pole-on orientation of its rotation axis

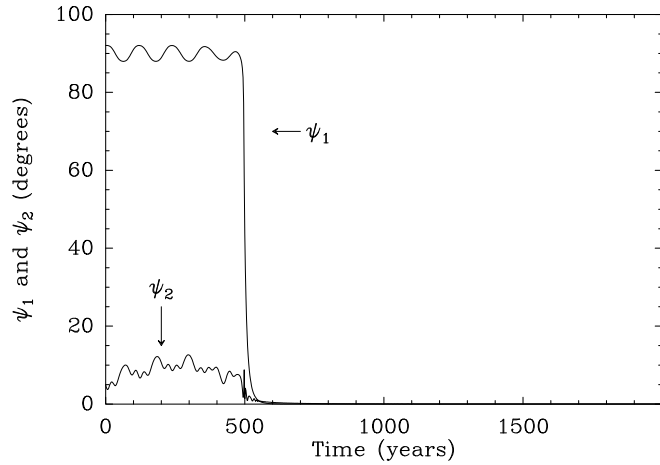


Fig. 20. Same as Fig. 13, but at t_{MS}

ics is responsible for this fact: a Kozai cycle is initiated, which enhances the tidal effects, and causes rapid synchronization and alignment.

5.3. Interpretation

In order to understand this peculiar behavior, one has to describe the variations of ψ_1 . From Eq. (36), we clearly have

$$-\sin(\psi_1) \frac{d\psi_1}{dt} = -D \frac{d\theta_1}{dt} - U \frac{di}{dt} + B \sin i \frac{d(\Omega - \phi_1)}{dt}, \quad (37)$$

where

$$D = \sin \theta_1 \cos i - \cos \theta_1 \sin i \cos(\phi_1 - \Omega); \quad (38)$$

$$U = \cos \theta_1 \sin i - \sin \theta_1 \cos i \cos(\phi_1 - \Omega); \quad (39)$$

$$B = \sin \theta_1 \sin(\phi_1 - \Omega). \quad (40)$$

In the present equation, one has to distinguish the terms arising from the classical tidal effects and those arising from the 3-body

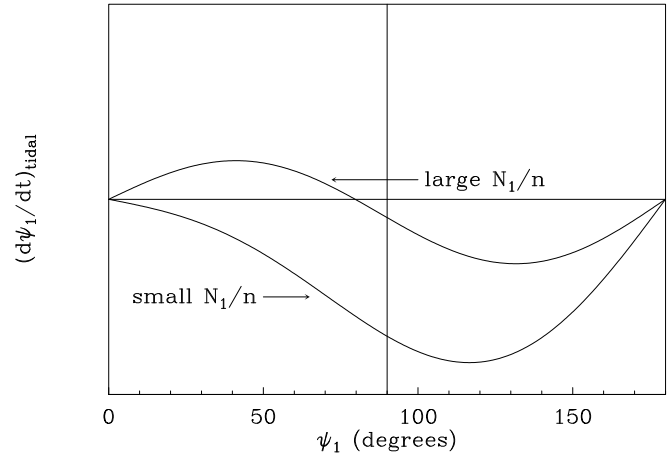


Fig. 21. $(d\psi_1/dt)_{\text{tidal}}$ (as defined by Eq. (42)) as a function of ψ_1 for various values of N_1/n

dynamics. The 3-body dynamics only acts on Ω and i , not on θ_1 nor on ϕ_1 . We may then write

$$-\sin \psi_1 \frac{d\psi_1}{dt} = \left(\frac{d\psi_1}{dt} \right)_{\text{tidal}} - U \left(\frac{di}{dt} \right)_{\text{3-body}} + B \sin i \left(\frac{d\Omega}{dt} \right)_{\text{3-body}}. \quad (41)$$

Let us now focus on the tidal terms and forget the 3-body contribution. The tidal contribution may be obtained combining the variation equations given by Alexander (1973). As ψ_1 does not depend on the referential frame used, its variations may be expressed as a function of ψ_1 only. If we assume $e = 0$ in the Alexander equations (the eccentricity of the binary orbit is small), and if we neglect the contribution of the $1.6 M_{\odot}$ secondary to the equations (this is a minor correction) we get finally

$$\left(\frac{d\psi_1}{dt} \right)_{\text{tidal}} = P n^2 \sin \psi_1 \left[Q \left(\cos \psi_1 - \frac{2n}{N_1} \right) - R \frac{N_1}{n} \right], \quad (42)$$

where P , Q and R are numeric coefficients given by

$$P = \frac{1}{4} T_1 \sum_{j=2}^4 (j+1) (k_j)_1 \left(\frac{R_1}{a} \right)^{2j+1}; \quad (43)$$

$$Q = \frac{m_2}{m_1 + m_2} \frac{m_2}{m_1} \frac{a^2}{R_1^2 g_1^2}; \quad (44)$$

$$R = \frac{m_2}{m_1}. \quad (45)$$

Here, T_1 stands for the constant time lag characteristic for the weak friction model. As explained above, in our calculations T_1 and T_2 are adjusted at every time in such a way that the characteristic time scales correspond to the Tassoul & Tassoul ones. Note that Q and R are purely dimensionless coefficients, while P has the dimension of a time. The behavior of ψ_1 under tidal effects depends actually on the value of N_1/n , i.e., the

rotation velocity of the primary relative to the orbital motion of the binary. This may be seen on Fig. 21, where the shape of $(d\psi_1/dt)_{\text{tidal}}$ as a function of ψ_1 is illustrated for various values of N_1/n . We first see that $\psi_1 = 0$ (i.e., alignment) is always an equilibrium point, and that it is a stable point for small values of N_1/n ; but for large enough values of N_1/n , that equilibrium becomes unstable, and a new stable points appears between 0 and 90° . The critical value of N_1/n separating the two regimes may be expressed as

$$\left(\frac{N_1}{n}\right)_{\text{critical}} = \frac{4}{1 + \sqrt{1 + 8R/Q}}. \quad (46)$$

In the case of the TY CrA system, this value is very close to 2, because we have $R \ll Q$. It may also be seen from Eq. (42) that for even higher values, the equilibrium points decreases again and finally, $\psi_1 = 0$ becomes a stable point again. In fact, there is a maximum value for the equilibrium point which is obtained for $N_1/n = \sqrt{2Q/R}$. In the case of the TY CrA system, this value of N_1/n is about 22, and the corresponding equilibrium point is close to 80° .

We may thus understand why when the primary is super-synchronous enough ($N_1/n \gtrsim 2$), the aligned position is no longer a stable point. However, as the maximum possible equilibrium value for ψ_1 is $\sim 80^\circ$, the 90° position revealed by Fig. 18 is still unexplained. That is why we come now to focus on the role of the 3-body terms. From Eq. (41), we see that these terms involve both $(d\Omega/dt)_{3\text{-body}}$ and $(di/dt)_{3\text{-body}}$. $(d\Omega/dt)_{3\text{-body}}$ (precession velocity) is roughly constant, while i also remains constant. $(di/dt)_{3\text{-body}}$ is then as an oscillating term; its temporal average is therefore close to zero, and it might be neglected with respect to $(d\Omega/dt)_{3\text{-body}}$. This may be however seen from the first order expansion of the 3-body Hamiltonian (21).

It is convenient to average once more Eq. (21) over ω which is a rapidly circulating argument. The averaged expression reduces to

$$\langle \overline{U_1} \rangle = \frac{\mu(1-\mu)\mu'(1-\mu')}{16(1-e^2)^{3/2}} \frac{a^2}{a'^3} (2+3e^2)(1-3x_1^2). \quad (47)$$

The precession velocity $d\Omega/dt$ is obtained from Eqs. (14) as

$$\left(\frac{d\Omega}{dt}\right)_{3\text{-body}} = \frac{1}{\rho} \frac{\partial U_1}{\partial \Theta} = -\frac{1}{\rho G \sin i} \frac{\partial U_1}{\partial i} \quad (48)$$

Taking the above averaged expression for U_1 , and assuming $\cos(\Omega - \Omega') \simeq -1$ (because $\Omega - \Omega' \simeq \pi$), we get

$$\left(\frac{d\Omega}{dt}\right)_{3\text{-body}} \simeq -\frac{3}{16} \frac{\mu\mu'}{\sqrt{1-\mu}} \frac{a^2}{a'^3} \sqrt{\frac{\mathcal{G}M}{a}} \times \frac{2+3e^2}{\sqrt{1-e^2(1-e'^2)^{3/2}}} \frac{\sin[2(i+i')]}{\sin i}. \quad (49)$$

The variations of i may be obtained the same way:

$$\left(\frac{di}{dt}\right)_{3\text{-body}} = \frac{1}{\rho G \sin i} \left(\frac{\partial U_1}{\partial \Omega} - \cos i \frac{\partial U_1}{\partial \omega} \right), \quad (50)$$

which finally reduces to

$$\left(\frac{di}{dt}\right)_{3\text{-body}} \simeq \frac{3}{8} \frac{\mu\mu'}{\sqrt{1-\mu}} \frac{a^2}{a'^3} \sqrt{\frac{\mathcal{G}M}{a}} \sin(\Omega - \Omega') \times \frac{2+3e^2}{\sqrt{1-e^2(1-e'^2)^{3/2}}} \sin i' \cos(i+i'). \quad (51)$$

We see that $(di/dt)_{3\text{-body}}$ contains a $\sin(\Omega - \Omega')$ factor, which is not the case for $(d\Omega/dt)_{3\text{-body}}$. $\Omega - \Omega'$ is close to π (see Fig. 12). Indeed, this last expression just shows that according to pure 3-body dynamics, the variations of i are higher order than those of Ω . We may therefore safely neglect $(di/dt)_{3\text{-body}}$ in Eq. (41).

The remaining 3-body term in Eq. (41) involves $(d\Omega/dt)_{3\text{-body}}$, which is roughly constant [this may be seen directly from Eq. (49)], and an angular factor, namely $-\sin \theta_1 \sin(\phi_1 - \Omega_1) \sin i / \sin \psi_1$. In the numerical experiment described in Figs. 17–19, this factor appears to be rapidly oscillating between $-\sin i$ and $\sin i$ around a zero mean. Hence the 3-body term in Eq. (41) is an oscillating term. Only its time-averaged effects must be taken into account. One has thus to focus on the temporal mean of this term.

To allow a correct description, we may introduce another angular parameter describing the position of the rotation axis of the primary. The direction of this axis is defined by ϕ_1 and θ_1 . We may also define it relatively to the angular momentum of the binary, i.e., by the tilt angle ψ_1 and a rotation angle η_1 around it. Of course, ψ_1 and η_1 are related to ϕ_1 and θ_1 , first by Eq. (36), and by the following relations:

$$\begin{cases} \cos \theta_1 = \cos i \cos \psi_1 - \sin \psi_1 \cos \eta_1 \sin i \\ \sin \theta_1 \cos(\phi_1 - \Omega) = \cos \psi_1 \sin i + \sin \psi_1 \cos \eta_1 \cos i \\ \sin \theta_1 \sin(\phi_1 - \Omega) = \sin \psi_1 \sin \eta_1 \end{cases} \quad (52)$$

Hence, Eq. (41) may be rewritten as follows:

$$\frac{d\psi_1}{dt} = \left(\frac{d\psi_1}{dt}\right)_{\text{tidal}} - \sin \eta_1 \sin i \left(\frac{d\Omega}{dt}\right)_{3\text{-body}}. \quad (53)$$

It is now interesting to describe the variations of η_1 , which may be obtained from the definition of $\sin \eta_1$. Combining the equations of Alexander (1973), and assuming $e = 0$ as for ψ_1 , we obtain after some algebra:

$$\frac{d\eta_1}{dt} = \left(\frac{R_1}{a}\right)^3 \frac{m_2 (k_2)_1 N_1}{2m_1 g_1^2} \cos \psi_1 - \frac{N_1 n P R \sin \psi_1 \sin \eta_1}{\tan i} - \left(\cos i + \frac{\sin i \cos \psi_1}{\cos \eta_1 \sin \psi_1} \right) \left(\frac{d\Omega}{dt}\right)_{3\text{-body}}, \quad (54)$$

where P and R are defined by Eqs. (43) and (45). In this equation, the first term represents the contribution of the rotational tidal effects (these terms cancel in the variations of ψ_1 but not for those of η_1), the second one is the lagging tide contribution, and the last one is the 3-body contribution.

The oscillating term in the 3-body part of Eq. (41) is then only $\sin \eta_1$. The temporal mean of this term may be assimilated

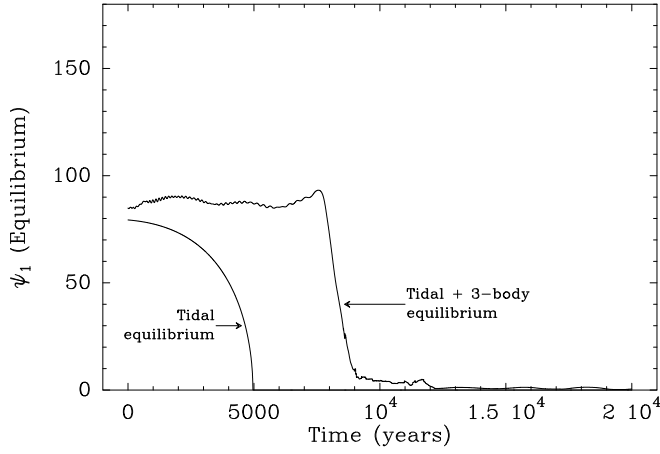


Fig. 22. Plot of the equilibrium value of ψ_1 as a function of time for the run corresponding to Figs. 17–19, obtained solving Eq. (41): i) neglecting the 3-body contribution ii) adding the 3-body contribution

to corresponding to the stationary point of Eq. (54). Hence the equilibrium point is found solving the right hands of Eqs. (53) and (54).

We may now compare the three terms of Eq.(54) in the peculiar case of TY CrA, at t_{PMS} :

- rotational term (s^{-1}): $\sim -3.8 \cdot 10^{-9} \frac{N_1}{n} \cos \psi_1$;
- lagging-tide term (s^{-1}): $\sim -5.2 \cdot 10^{-14} \frac{N_1}{n} \frac{\sin \psi_1 \sin \eta_1}{\tan i}$;
- 3-body term: $\left(\frac{d\Omega}{dt} \right)_{3\text{-body}} \simeq 7 \cdot 10^{-11} \text{s}^{-1}$ [Eq. (49)].

The lagging-tide term is thus negligible compared to the first one.

This holds also for Eq. (53), where $(d\psi_1/dt)_{\text{tidal}} \ll (d\Omega/dt)_{3\text{-body}}$. Hence we must have $\sin \eta_1 \simeq 0$ at equilibrium. From Eq. (54), and neglecting the lagging-tide contribution, we derive at equilibrium:

$$\sin \psi_1 \left(y - \frac{\cos i}{\cos \psi_1} \right) = \frac{\sin i}{\cos \eta_1} \simeq \pm \sin i \quad (55)$$

where

$$y = \left(\frac{R_1}{a} \right)^3 \frac{m_2 (k_2)_1 N_1}{2m_1 g_1^2 (d\Omega/dt)_{3\text{-body}}} \simeq 54 \frac{N_1}{n} \text{ at } t_{\text{PMS}}. \quad (56)$$

Depending on the sign of $\cos \eta$, there are one or three roots between 0 and π to Eq. (55). In any case, there is only one stable root which is close to 90° . For $N_1/n > 1$ the solution is in any case closer to 90° than 0.2° . Hence we understand why the equilibrium is shifted to 90° by the 3-body dynamics. In fact, the equilibrium is mainly due to the 3-body term of Eq. (53) which dominates the tidal term. As a final test, Fig. 22 plots the solution of the equilibrium equation of ψ_1 as a function of time. Equation (41) is solved at every time with the corresponding values taken from the run illustrated by Figs. 17–19. The lower curve is obtained solving the tidal part of Eq. (41) only, while for

the upper curve, the complete equation was taken into account. For the 3-body term, a running average over 400 yrs was taken. The difference between the two curves illustrates the shifting effect of the 3-body dynamics on the equilibrium. Moreover, with the 3-body dynamics, this pseudo-equilibrium is maintained for a longer time than with pure tidal effects. Finally, the similarity with Fig. 18 is striking, illustrating the validity of the theory described above.

6. Long-term evolution of the TY CrA system

The theory described in the previous section appears indeed well suited to explain the apparent non-synchronism of the central binary of TY CrA. The 3-body dynamics enhances a pseudo-equilibrium constraining the rotation axis of the $3.0 M_\odot$ primary to the orbital plane of the binary. However, we see from Fig. 18 that in any case, the duration of this phase should not exceed $\sim 10\,000$ years. Even if the age of the TY CrA system is unknown, this is a very short duration, and one should expect the TY CrA system to be synchronized today. In fact, if we assume the values given by Table 4 for the characteristic times of the meridional circulation model by Tassoul & Tassoul (1992), there is no way to explain a non-synchronism of the binary after at most 10^5 years. One has then to admit that these constants are significantly smaller in the peculiar case of the central binary of the TY CrA system. This might be justified by the fact that all characteristic times for various tidal effects highly depend on the internal viscosity of the star, which is in any case very poorly known, and just estimated to derive the characteristic times.

In order to test this theory, we decided to investigate the dynamics of TY CrA over a longer time-scale (a few 10^7 yrs), with significantly reduced Tassoul constants. Compared to the previous runs, we had to take into account the fact that the internal structure of the stars may evolve over such a time-scale. More precisely, we cannot assume that the radii, gyration radii, apsidal constants, etc. . . of the stars are constant over the integration. This is why we decided to introduce the calculation of these quantities at every time during the integration, using the models by Siess et al. (1996) with $Z = 0.02$. In order to spare computing time, we also decided to use the expanded expression (21) for the perturbative 3-body potential, instead of the numerical integration of the full Hamiltonian (17). Besides, we tested this simplified version with the same initial conditions as for all the previous runs computed with the numerical integration. Apart from minor changes (a few percent in the time-scales), the results are identical. In particular, i) the global circularization/synchronization process is not affected by this approximation, ii) the Kozai mechanism is preserved when it is present and iii) the marginal equilibrium with $\psi_1 \simeq 90^\circ$ is also preserved over the same time-scale.

Starting from various initial conditions at $t \simeq 0$, we integrated the dynamics of the TY CrA system over a few 10^7 yrs, with evolving stars, and reduced Tassoul & Tassoul tidal effects. It can be seen from Fig. 7 that 10^7 yrs corresponds roughly to the pre main sequence phase for the $1.6 M_\odot$ secondary. Our aim was mainly to investigate the long-term stability of the marginal

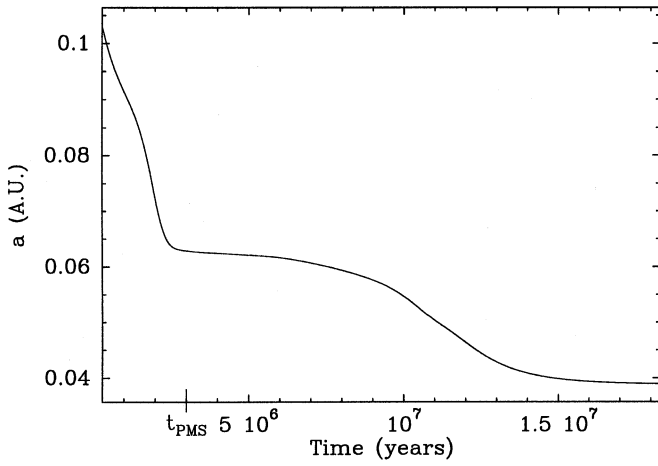


Fig. 23. Long-term evolution of the semi-major axis of the central binary under tidal effects, with reduced Tassoul constants, for $1.8 \cdot 10^7$ yrs. The semi-major axis regularly decreases. The value at t_{PMS} corresponds roughly to the present value (see Fig. 8)

$\psi_1 = 90^\circ$ equilibrium, so that we gave this initial value to ψ_1 . Apart from this, we did not want to reproduce exactly the present orbital configuration of the TY CrA system at a given age (e.g., t_{PMS}), as most of the angular orbital parameters (longitude of nodes, arguments of periastra, etc. . .) are subject to circulation over a time-scale of a few 10^3 yrs at most, which is far less than the error bar on the present age of TY CrA. However, some of the initial parameters at $t = 0$ appeared to have a crucial role for the future evolution, namely i) the initial semi-major axis of the binary ii) the reduction factor applied to the Tassoul constants and iii) the initial rotation velocities of the stars.

Concerning the initial separation of the binary, it is quite intuitive to guess its role: first, taking an too small initial value leads rapidly to a collapse of the central binary; second, assuming a too large value (thus significantly reducing *all* tidal effects) allows the 3-body dynamics to initiate a large amplitude Kozai cycle, leading either to a rapid circularization/synchronization, either to a collapse of the central binary. Indeed, it appeared that in order to avoid these two extreme pictures, we had to choose the initial semi-major axis a of the binary in the range 1.5 – 2 times its present value, i.e., ~ 0.1 U.A.. All the integrations using such an initial value showed a long-term decrease of a from $t = 0$ to reach a value roughly corresponding to the present one at t_{PMS} .

The reduction factor applied to the Tassoul effects is of course crucial for the circularization time-scales. However, we may stress that we cannot apply an arbitrarily small reduction factor. Indeed, if this factor is less than ~ 3000 , the Tassoul & Tassoul effects becomes weaker than the dynamical tide effect (see Table 4) which should then be taken into account. We thus considered this value as an upper limit.

Figures 23–25 show the result of an integration with such initial conditions for $1.4 \cdot 10^7$ yrs. The reduction factor applied to the Tassoul effect is 400, and the initial semi-major axis is 1.6 times the present value. We see that the binary gradually

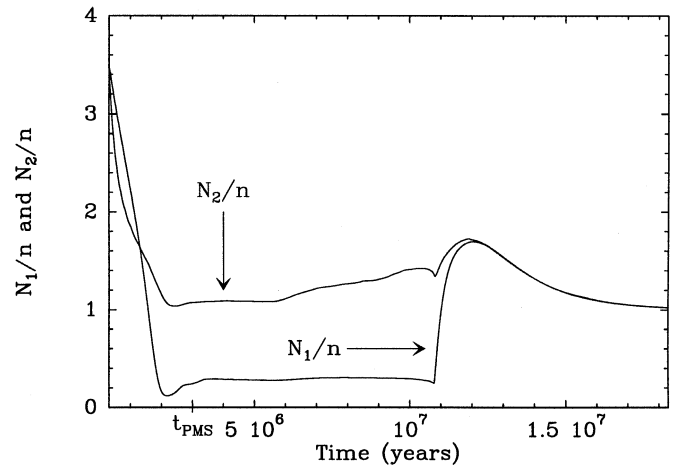


Fig. 24. Same as Fig. 23, but for the rotation velocities of the binary components. Both stars are initially supersynchronous, but a gradual slow-down process is detected. The stars quickly synchronize after 10^7 yrs. Note that the primary remains significantly subsynchronous for a long time

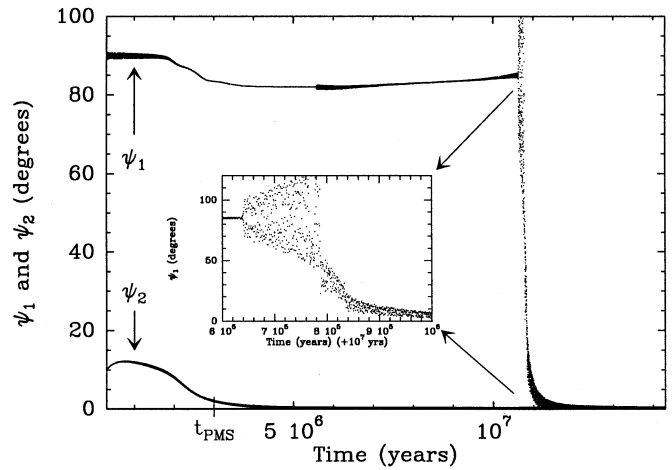


Fig. 25. Same as Fig. 23, but for the tilt angles ψ_i ($i = 1, 2$). The rotation axis of the primary remains constrained to the precessing orbital plane of the binary for $\sim 1.1 \cdot 10^7$ yrs. The central inner plot is an enlargement of the transition epoch for ψ_1 between $\sim 90^\circ$ and $\sim 0^\circ$. The alignment is achieved within a few 10^5 yrs

synchronizes over this time-scale, while the rotation axes remain constrained to the precessing orbital plane of the binary for a few million years before aligning. This behavior is similar to that of Figs. 17–19, but the time-scale is much longer. In particular, we note that the marginal equilibrium is maintained up to $\sim 10^7$ yrs, and that the binary synchronizes very quickly afterwards. Moreover, testing other initial conditions (Tassoul reduction factor and/or initial value of the semi-major axis) revealed that, whenever the marginal equilibrium is maintained, it is always broken suddenly at a time of the order of 10^7 yrs. This must not be surprising, since according to Fig. 7, 10^7 yrs corresponds to the time when both components of the primary

have roughly reached the main sequence, i.e., when the tidal effects are weaker.

It is interesting to note that we do not need to assume high initial rotation velocities for both components (Fig. 24). This is clearly due to the fact that the internal structure of the stars changes during the integration. Indeed, when a radiative core grows at the center of a star, its gyration radius drops (the star becomes more compact), and if its angular momentum was conserved, one should expect its rotation velocity to increase. Here, this effect is not strong enough to overcome the tidal synchronization process which makes the rotation of the stars decrease, but it slows it significantly.

7. Interpretation

The long-term run shows that the survival of the marginal equilibrium characterized by $\psi_1 \simeq 90^\circ$ (and also possibly ψ_2 ; we have tested runs where both components were initially chosen at $\psi \simeq 90^\circ$, and where this value was maintained for both stars for a long time) is able to last several 10^6 yrs long, provided the tidal effects are not too strong. If we assume that the present age of TY CrA is $t_{\text{PMS}} \simeq 3 \cdot 10^6$ yrs, this situation could still be valid today. However, it is unrealistic to imagine that the marginal equilibrium could still survive at t_{MS} . First, Fig. 20 shows clearly that when both components of the binary are on the main sequence, thanks to the 3-body dynamics, the synchronization and alignment occur on a much more rapid time-scale. Moreover, this would require the marginal equilibrium to last for more than 10^8 yrs, which is a more constraining condition.

We may therefore suggest that i) the present age of TY CrA is probably t_{PMS} rather than t_{MS} (this is already suggested by Fig. 1) and ii) the present status of the rotation axes of the binary corresponds to the marginal equilibrium, at least for the $3.0 M_\odot$ primary. This requires the Tassoul & Tassoul tidal mechanism to be in the case of TY CrA significantly smaller than usually. Nevertheless, if this effect was really as strong as predicted, one should expect the central binary to be already synchronized, even at t_{PMS} , which does not match the observations.

We stress however that the marginal equilibrium configuration may fit the present observational rotational characteristics of TY CrA. Indeed, the observed $v \sin i$ (8 km s^{-1} , Paper I) of the primary suggests that either its rotation is subsynchronous, either its rotation axis is not aligned with the angular momentum of the primary. The marginal equilibrium might explain the non-alignment. However, this would require this star to be seen nearly pole-on to make its $v \sin i$ to be small enough. This constraint may be evaluated. It can be seen from Fig. 18 that the survival of the marginal equilibrium requires $N_1/n \lesssim 0.4$. In fact, the long-term integration shows that it is maintained for several million years with $N_1/n \simeq 0.3$. If we call α this limiting ratio, and v_0 the equatorial velocity which would correspond to synchronism, the inclination angle i with respect to the line of sight must obviously satisfy

$$\sin i > \frac{w}{\alpha v_0}, \quad (57)$$

if w is the measured $v \sin i$. If we assume that the direction of the rotation axis of the primary is randomly distributed over a sphere, the probability of such an occurrence is

$$P = 1 - \sqrt{1 - \left(\frac{w}{\alpha v_0}\right)^2}. \quad (58)$$

With $\alpha = 0.3$, $w = 8 \text{ km s}^{-1}$ and $v_0 = 46 \text{ km s}^{-1}$, we have $P = 18.5\%$. This is still acceptable, but if we assume $\alpha = 1$, we have now $P = 1.5\%$ which is too small to be realistic.

In fact, one should recall that in the frame of the marginal equilibrium, the rotation axis of the primary cannot be randomly distributed on a sphere, but it is constrained to lie in the orbital plane of the binary ($\psi_1 = 90^\circ$). Moreover, this is still compatible with a pole-on location, since the line of sight lies in the orbital plane (TY CrA is an eclipsing binary). Therefore, the orientation of the rotation axis of the primary should be taken randomly distributed *within a plane* rather than in space. Taking this into account, the probability now becomes

$$P = \frac{2}{\pi} \arcsin\left(\frac{w}{\alpha v_0}\right). \quad (59)$$

With $\alpha = 0.3$, we have now $P = 39.4\%$ which is very high, and with $\alpha = 1$ we still have $P = 11.1\%$. It thus appears that the ‘‘pole-on’’ condition is not very strong, and could easily be satisfied.

8. Conclusion

We have investigated the dynamics of the triple stellar system TY CrA, focusing on the coupling between the 3-body dynamics and the tidal effects inside the central binary. The stability of the system first appears ensured by tidal effects. Indeed, without any tidal process, the 3-body dynamics should make the central binary collapse rapidly. Taking tidal effects into account, we have shown that despite the rapid precession of the orbital plane of the binary, its equilibrium configuration is characterized by corotation, axes alignment, and circularization. However, we have seen that thanks to the precession of this plane (due to the interaction with the third component), a marginal equilibrium for the components of the binary appears, characterized by a confinement of the rotation axes to its orbital plane. We stress that this peculiar equilibrium could correspond to the present status of TY CrA, at least for the $3.0 M_\odot$ primary. This would indeed explain its apparent subsynchronism as a consequence of non-alignment of the rotation axis with the orbital angular momentum. However, this is only possible if TY CrA is only a few 10^6 yrs old, i.e. if its present age is t_{PMS} rather than t_{MS} , which was also suggested by the analysis of the evolutionary tracks (Fig. 1), even if it was impossible to definitely make a choice between t_{PMS} and t_{MS} on this mere basis. The dynamical analysis makes the choice possible because the internal structure of the $1.6 M_\odot$ secondary is drastically different at t_{PMS} and t_{MS} . We nevertheless need the tidal effects to be significantly smaller than predicted by Tassoul & Tassoul (1992), otherwise

the central binary should have already synchronized, which is obviously not compatible with the observations. We think that this is not in itself a very strong constraint, since the values of the corresponding characteristic times are not very strongly constrained, as they depend on parameters which may vary among various stars.

The 3-body dynamics is responsible for the precession of the orbital plane of the central binary, over a time-scale of a few 10^3 yrs. This has a first important consequence: the central binary of the TY CrA system will not remain an eclipsing one. Indeed, the present eclipsing situation is fortuitous, but it is expected to evolve within ~ 100 yrs.

This new picture may also provide clues for understanding the problem of the circumstellar material around TY CrA. Lagrange et al. (Paper I) reported that all the spectroscopic absorption they detected in the spectrum of TY CrA exhibit periodic radial velocity variations, and could not correspond to circumbinary material. However, the detection of a strong infrared excess toward TY CrA (Cruz-Gonzalez et al. 1984; Wilking et al. 1985) attributed to circumstellar grains leads to think that some circumstellar material is present around TY CrA. As the binary is eclipsing the gaseous counterpart of the circumbinary dust was expected to be detected spectroscopically in absorption. However, we may stress now that there is probably no circumbinary disk. Indeed, the rapid precession of its orbital plane should prevent the formation of such a disk. However, as seen in Sect. 3, the orbital plane of the third component is much more stable. Therefore, if some circumstellar material was present, one should expect to find it in a circumtertiary disk, located in the orbital plane of the tertiary. Of course, such a disk should be affected by the 3-body dynamics (waves, warp. . .), but in any case, it should not lie in the orbital plane of the binary. As the orbital plane of the third component does not contain the line of sight, we would thus explain the non detection of the gaseous counterpart of the circumstellar dust around TY CrA.

References

- Alexander M.E., 1973, Ap&SS 23, 459
 Bailey M.E., Chambers J.E., Hahn G., 1992, A&A 257, 315
 Bibo E.A., Thé P.S., Dawanas D.N., 1992, A&A 260, 293
 Brooker R.A., Olle T.W., 1955, MNRAS 115, 101
 Casey B., Mathieu R.D., Suntzeff N., Lee C.-W., Cardelli J.A., 1993, AJ 105, 2276
 Casey B., Mathieu R.D., Suntzeff N., Walter F.M., 1995, AJ 109, 2156
 Corporon P., Lagrange A.-M., Bouvier J., 1994, A&A 282, L21
 Corporon P., Lagrange A.-M., Beust H., 1996, A&A 310, 228
 Cruz-Gonzalez I., McBreen B.P., Fazio G.G., 1984, ApJ 279, 679
 Duriez L., 1989, in *Les méthodes modernes de la mécanique céleste*, D. Benest and C. Froeschlé, Eds., Frontières, p. 1
 Hale A., 1994, AJ 107, 306
 Hut P., 1980, A&A 92, 167
 Hut P., 1981, A&A 99, 126
 Hut P., 1982, A&A 110, 37
 Kardopolov V.I., Sahanionok V.V., Phylipjev G.K., 1981, Perem. Zvezdy 21, 589
 Koch R.H., Hvrinak B.J., 1981, AJ 86, 438
 Kopal Z., 1978, Dynamics of close binary systems, Reidel, Dordrecht
 Kozai Y., 1962, AJ 67, 591
 Lagrange A.-M., Corporon P., Bouvier J., 1993, A&A 274, 785

- Laskar J., 1989, in *Les méthodes modernes de la mécanique céleste*, D. Benest and C. Froeschlé, Eds., Frontières, p. 63
 Lestrade J.F., Phillips R.B., Hodges M.W., Preston R.A., 1993, ApJ, 410, 808
 Mathieu R.D., Mazeh T., 1988, ApJ 326, 256
 Mayor M., Mermilliod, J.-C., 1984, *Observational Tests of the Stellar Evolution Theory*, eds. A. Maercker, A. Renzini, Reidel, Dordrecht, p. 411
 Moons M., 1993, *Rapport interne du département de mathématique FUNDP*, Namur, Belgium
 Moons M., 1994, Celest. Mech. 60, 173
 Press W.H., Wiita P.J., Smarr L.L., 1975, ApJ 202, L135
 Siess L., Forestini M., Dougados C., 1997, submitted
 Tassoul J.-L., Tassoul M., 1992, ApJ 395, 259
 Wilking B.A., Harvey P.M., Joy M., Hyland A.R., Jones T.J., 1985, ApJ 293, 165
 Zahn J.-P., 1975, A&A 41, 329
 Zahn J.-P., 1977, A&A 57, 383